DISEASES AND DISORDERS

Galectin-1 prevents pathological vascular remodeling in atherosclerosis and abdominal aortic aneurysm

Raquel Roldán-Montero[1,2], Juan M. Pérez-Sáez[3], Isabel Cerro-Pardo[1], Jorge Oller[4,5], Diego Martinez-Lopez[1], Estefania Nuñez[6], Sebastian M. Maller[3], Carmen Gutierrez-Muñoz[1], Nerea Mendez-Barbero[1,2], Joan C. Escola-Gil[7,8], Jean-Baptiste Michel[9], Maria Mittelbrunn[4,5], Jesús Vázquez[2,6], Luis M. Blanco-Colio[1,2], Gabriel A. Rabinovich[3,10]*†, Jose L. Martin-Ventura[1,2]*†

Pathological vascular remodeling is the underlying cause of atherosclerosis and abdominal aortic aneurysm (AAA). Here, we analyzed the role of galectin-1 (Gal-1), a β-galactoside–binding protein, as a therapeutic target for atherosclerosis and AAA. Mice lacking Gal-1 (*Lgals1*$^{-/-}$) developed severe atherosclerosis induced by pAAV/D377Y-mPCSK9 adenovirus and displayed higher lipid levels and lower expression of contractile markers of vascular smooth muscle cells (VSMCs) in plaques than wild-type mice. Proteomic analysis of *Lgals1*$^{-/-}$ aortas showed changes in markers of VSMC phenotypic switch and altered composition of mitochondrial proteins. Mechanistically, Gal-1 silencing resulted in increased foam cell formation and mitochondrial dysfunction in VSMCs, while treatment with recombinant Gal-1 (rGal-1) prevented these effects. Furthermore, rGal-1 treatment attenuated atherosclerosis and elastase-induced AAA, leading to higher contractile VSMCs in aortic tissues. Gal-1 expression decreased in human atheroma and AAA compared to control tissue. Thus, Gal-1–driven circuits emerge as potential therapeutic strategies in atherosclerosis and AAA.

INTRODUCTION

Cardiovascular (CV) diseases are the leading cause of global mortality and a major contributor to disability (*1*). Among them, atherosclerosis and aortic aneurysms are characterized by a pathological remodeling of the vascular wall that could progress to plaque and/or aortic wall rupture and eventually to CV events and/or deaths. Treatment of both atherosclerosis and aneurysms is only based on the control of different CV risk factors, highlighting the need to find potential therapeutic targets to prevent the devastating effects of vascular rupture (*2*).

The main driver of atherosclerosis is lipid retention and modification, mainly by oxidation, leading to foam cell formation, which characterizes the early atherosclerotic lesions. Progression to intermediate fibrolipidic lesions is fueled by different processes, including phenotypic modulation of vascular smooth muscle cells (VSMCs) characterized by decreased contractile function, higher proliferative activity, and increased extracellular matrix (ECM) production (*3*). Last, failure of resolution programs, engagement of cell death pathways leading to necrotic core formation, and degradation of ECM favor the instability of atherosclerotic plaques and facilitate their rupture (*4*). Abdominal aortic aneurysm (AAA) shares many of these pathological processes, with a predominant role of proteolysis. Proteases released by infiltrating or resident cells may degrade elastin and other ECM proteins, which, along with VSMC loss, favor aortic dilation and potential rupture (*5*).

Galectins, a family of ancient β-galactoside–binding proteins, can reprogram immune and vascular programs through intracellular and extracellular mechanisms (*6*). Intracellularly, galectins can regulate signaling pathways, innate defense mechanisms, and splicing. Extracellularly, they can elicit various cellular responses through glycan-dependent circuits, including modulation of cytokine production, cell adhesion, angiogenesis, and cell death (*7*). Through these mechanisms, galectins can control inflammation, wound healing, antimicrobial immunity, and tumor-immune escape (*6*–*8*). Specifically, galectin-1 (Gal-1), a prototype member of the galectin family, promotes resolution of acute and chronic inflammation by recalibrating innate and adaptive immune responses via glycosylation-dependent pathways (*9*, *10*). However, despite considerable progress in elucidating the role of Gal-1 in immunopathology (*7*), its contribution to CV diseases is just emerging (*11*). Mice lacking Gal-1 showed enhanced cardiac inflammation during acute myocardial infarction (AMI), and administration of recombinant Gal-1 (rGal-1) attenuated AMI-associated inflammatory responses (*12*).

In this study, we identify a central role of Gal-1 in atherosclerotic plaque size, burden, and stability in vivo through mechanisms involving modulation of foam cell formation and mitochondrial functionality associated to VSMC phenotypic switch. Moreover, we demonstrate the potential therapeutic role of rGal-1 in both atherosclerosis and AAA. In addition, we validate the relevance of Gal-1 in human vascular pathologies by investigating its regulated expression in human atherosclerotic plaques and AAA lesions.

RESULTS

Gal-1 limits development of atherosclerosis

To study the relevance of Gal-1 in chronic vascular pathologies, we first analyzed Gal-1 expression, at both the mRNA and protein levels, in human atherosclerotic plaques compared with healthy aortic

[1]IIS-Fundación Jiménez-Díaz-Autonoma University of Madrid (UAM). Madrid, Spain. [2]CIBER de Enfermedades Cardiovasculares (CIBERCV), Madrid, Spain. [3]Laboratorio de Glicomedicina, Instituto de Biología y Medicina Experimental (IBYME), Consejo Nacional de Investigaciones Científicas y Técnicas (CONICET), C1428ADN Buenos Aires, Argentina. [4]Centro de Biología Molecular Severo Ochoa, Centro Superior de Investigaciones Científicas-UAM, Madrid, Spain. [5]Instituto de Investigación del Hospital 12 de Octubre, Madrid, Spain. [6]Centro Nacional de Investigaciones Cardiovasculares Carlos III, Madrid, Spain. [7]IIB Sant Pau, Barcelona, Spain. [8]CIBERDEM, Madrid, Spain. [9]Inserm U1148, Paris, France. [10]Facultad de Ciencias Exactas y Naturales, Universidad de Buenos Aires, C1428AGE Buenos Aires, Argentina.
*Corresponding author. Email: jlmartin@fjd.es (J.L.M.-V.); gabyrabi@gmail.com (G.A.R.)
†These authors contributed equally to this work as co-senior authors.

wall samples. Gal-1 staining was prominent in the tunica media of control aortas mainly composed of α-smooth muscle actin (α-SMA)–positive VSMCs, while it was markedly decreased in human atherosclerotic plaques (Fig. 1A). Decreased *LGALS1* and α-*SMA* mRNA was verified by quantitative polymerase chain reaction (qPCR) analysis of human atherosclerotic plaques (Fig. 1, B and C). In addition, secreted Gal-1 was also decreased in conditioned medium from atherosclerotic plaques when compared to control aortas (Fig. 1D).

To investigate the role of endogenous Gal-1 in atherosclerosis, we analyzed the effect of Gal-1 deletion in a hyperlipidemic model of advanced atherosclerosis induced by pAAV/D377Y-mPCSK9 adenovirus injection along with high-fat diet for 16 weeks (*13*). We first performed a pilot study in wild-type (WT) versus *Lgals1*$^{-/-}$ mice ($n = 5$ each group) and analyzed the atherosclerotic burden by enface analysis of the whole aorta. As observed by oil red O (ORO) staining, *Lgals1*$^{-/-}$ mice showed a 164% increase of lesion area of the aorta as compared to WT mice (Fig. 1E). We then performed a larger experiment in WT ($n = 10$) and *Lgals1*$^{-/-}$ ($n = 12$) mice under the same experimental conditions. No differences were observed in body weights between both genotypes at the end of the experiment [WT = 33.9 ± 1.0 g versus *Lgals1*$^{-/-}$ = 35.8 ± 0.9 g, P = not significant (NS)]; however, increased levels of total cholesterol and very low density lipoprotein (VLDL) and low-density lipoprotein (LDL) cholesterol were observed in sera from mice lacking Gal-1 (fig. S1).

To further study the effects of Gal-1 deletion in serum cholesterol levels, we analyzed mRNA expression of the main receptors involved in LDL and VLDL clearance. No significant differences in mRNA expression of both receptors (*Ldlr* or *Vldlr*) could be observed in liver homogenates of different mouse strains (fig. S1). To gain further mechanistic insights, we next performed an unbiased proteomic study of liver homogenates from WT and *Lgals1*$^{-/-}$ mice. Enrichment analysis of the biological processes that were significantly altered [false discovery rate (FDR) < 5%] between these genotypes revealed subtle changes in heme-binding proteins (e.g., cytochrome c and hemopexin); however, we did not observe any major alteration in key proteins involved in cholesterol biosynthetic pathways (fig. S1).

To further elucidate possible mechanisms underlying the role of endogenous Gal-1 in CV pathology, we compared atherosclerotic lesion size in the aortic root in *Lgals1*$^{-/-}$ versus WT mice. Gal-1–deficient mice exhibited significantly increased plaque size compared with their WT counterpart (Fig. 1F). Moreover, as plaque composition is a main determinant of atherosclerosis progression and rupture, we then analyzed different markers of plaque instability including lipids and collagen content, necrotic core size, as well as α-SMA and CD68 expression in atherosclerotic plaques. Mice lacking Gal-1 exhibited higher lipid content in lesions compared with WT mice (Fig. 2A), while no significant changes were observed in the necrotic core area (Fig. 2B) or collagen content (Fig. 2C) between both genotypes. Expression of α-SMA and calponin (two markers of contractile VSMCs) was

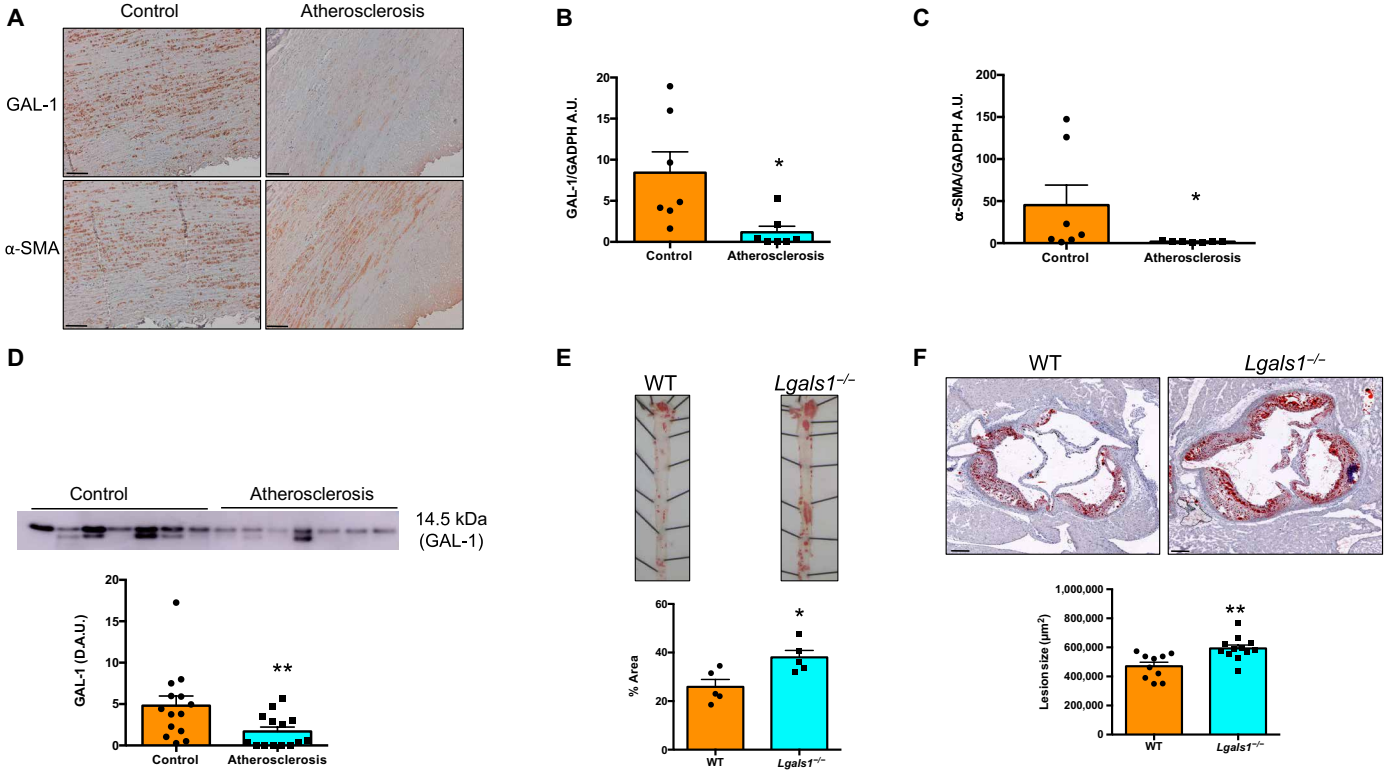

Fig. 1. Endogenous Gal-1 controls development of atherosclerosis. (**A**) Representative immunohistochemistry of GAL-1 in atherosclerotic plaques and healthy aortas. Scale bars, 100 μm. (**B**) Determination of *LGALS1* and (**C**) α-*SMA* mRNA in atherosclerotic plaques (intima layer, $n = 7$) versus healthy human control aortic samples (media layer, $n = 7$). (**D**) Western blot analysis of GAL-1 in atherosclerotic plaques (intima layer, $n = 14$) and healthy aortic (media layer, $n = 14$) tissue-conditioned medium. (**E**) Representative ORO staining in the whole aorta of WT ($n = 5$) and *Lgals1*$^{-/-}$ ($n = 5$) mice harvested at 16 weeks of AAV-PCSK9 infection and high-fat diet. (**F**) Representative ORO/hematoxylin staining in aortic root of WT ($n = 10$) and *Lgals1*$^{-/-}$ ($n = 12$) mice at 16-week harvest after AAV-PCSK9 infection and high-fat diet. Scale bars, 200 μm. Data are means ± SEM. *$P < 0.05$ or **$P < 0.01$, Mann-Whitney U test. D.A.U., densitometric arbitrary units.

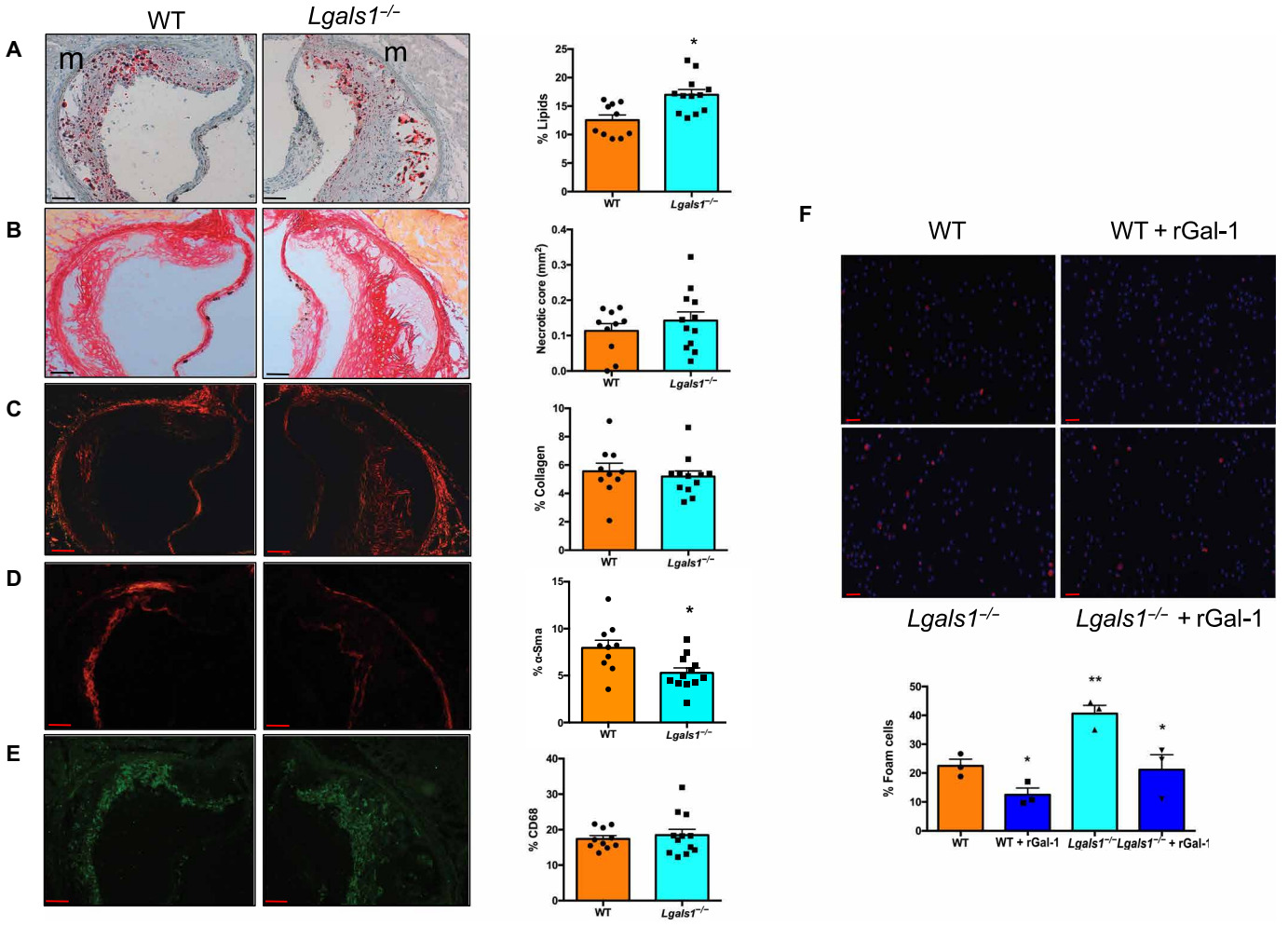

Fig. 2. Gal-1 deletion increases atherosclerotic plaque instability. Representative photographs and quantification of ORO (**A**), Sirius red [bright field (**B**) and polarized (**C**)], α-SMA (**D**), and CD68 (**E**) staining in the aortic root from WT ($n = 10$) and *Lgals1*$^{-/-}$ ($n = 12$) mice. Values are means ± SEM. *$P < 0.05$, Mann-Whitney *U* test. m, media layer. Scale bars, 100 μm. (**F**) Representative images and quantification of peritoneal macrophages isolated from WT or *Lgals1*$^{-/-}$ mice and incubated with Dil-oxidized LDL (10 μg/ml) for 4 hours with or without rGal-1 (1 μg/μl; 4-hour preincubation). Data are means ± SEM of three independent experiments. *$P < 0.05$, WT versus WT + rGal-1 or *Lgals1*$^{-/-}$ versus *Lgals1*$^{-/-}$ + rGal-1; **$P < 0.01$, *Lgals1*$^{-/-}$ versus WT, ANOVA test followed by Tukey's test. Scale bars, 50 μm.

substantially reduced in *Lgals1*$^{-/-}$ compared with control mice (Fig. 2D and fig. S2), while CD68 staining was similar in both mouse genotypes (Fig. 2E). To gain further insights into the mechanisms underlying higher lipid retention inside the vascular wall of atherosclerotic Gal-1–deficient mice, and given the association of ORO–positive cells with CD68^{+} cells (Fig. 2, A and E), we analyzed the ability of isolated peritoneal macrophages from *Lgals1*$^{-/-}$ and WT mice to take up fluorescently labeled Dil-oxidized LDL (10 μg/ml, 4 hours). An increased number of Gal-1–deficient macrophages accumulated greater lipid content as compared to WT macrophages (Fig. 2F). Moreover, treatment with rGal-1 (1 μg/ml; 4-hour preincubation) prevented increased Dil-oxidized LDL uptake elicited by either Gal-1–deficient or WT macrophages (Fig. 2F). Thus, Gal-1 controls the severity of atherosclerosis and influences lipid content and foam cell formation.

Gal-1 controls mitochondrial function and phenotypic switch of VSMCs

Given the atheroprotective effect of Gal-1, we performed a global proteomic approach in aorta homogenates from *Lgals1*$^{-/-}$ and WT mice. Enrichment analysis of the biological processes that were significantly changed (FDR < 5%) revealed two major pathways differentially regulated in aorta of WT versus *Lgals1*$^{-/-}$ mice, including up-regulation of cell adhesion pathways and down-regulation of lipid metabolic processes (Fig. 3A). In addition, enrichment analysis of cellular components revealed up-regulation of extracellular space mediators and down-regulation of mitochondrial proteins (fig. S3). Integrated analysis of biological processes and cellular components revealed a decrease of several proteins implicated in mitochondrial structure and function. To further investigate a possible direct effect of Gal-1 deletion in the expression of these genes, primary culture VSMCs were transfected with Gal-1 small interfering RNA (siRNA) (~50 to 70% of *Lgals1* mRNA reduction). Consistent with the proteomic data, *mt-Nd6* and *Nampt* mRNA expression was down-regulated in Gal-1–silenced VSMCs (Fig. 3B). Notably, MT-ND6 together with MT-ND1-5 are subunits of the NADH (reduced form of nicotinamide adenine dinucleotide) dehydrogenase (ubiquinone), an enzyme also known as complex I (*14*). In agreement, both *mt-Nd1* mRNA expression and complex I activity were also decreased in Gal-1–silenced VSMCs (Fig. 3B).

A

Category	Proteins	WT KO	ΔZq	P value
Cell adhesion	Fibronectin		2.585	0.049
	Vascular cell adhesion protein 1		2.318	0.011
	Insulin-like growth factor-binding protein 7		1.977	0.009
	Lactadherin		1.605	0.035
	Filamin-binding LIM protein 1		1.296	0.025
	Collagen alpha-1(XV) chain		1.210	0.023
Lipid metabolism	Nicotinamide phosphoribosyltransferase		−0.702	0.026
	Leucine-rich PPR motif–containing protein, mitochondrial		−0.702	0.047
	Complex I assembly factor ACAD9, mitochondrial		−0.773	0.005
	Dehydrogenase/reductase SDR family member 7B		−0.861	0.038
	Acetyl-coenzyme A synthetase, cytoplasmic		−0.968	0.014
	Catechol O-methyltransferase		−1.010	0.012
	Alpha-aminoadipic semialdehyde dehydrogenase		−1.123	0.016
	Long-chain-fatty-acid–CoA ligase 5		−1.201	0.040
	NADH dehydrogenase [ubiquinone] 1 alpha subcomplex subunit 6		−1.249	0.032
	Histidine triad nucleotide–binding protein 2, mitochondrial		−1.360	0.035
	Glycogen phosphorylase, liver form		−1.445	0.007
	NAD(P) transhydrogenase, mitochondrial		−1.564	0.019
	Acetyl-CoA carboxylase 1		−1.942	0.007
	ATP-citrate synthase		−2.162	0.049
	Fatty acid synthase		−3.098	0.038

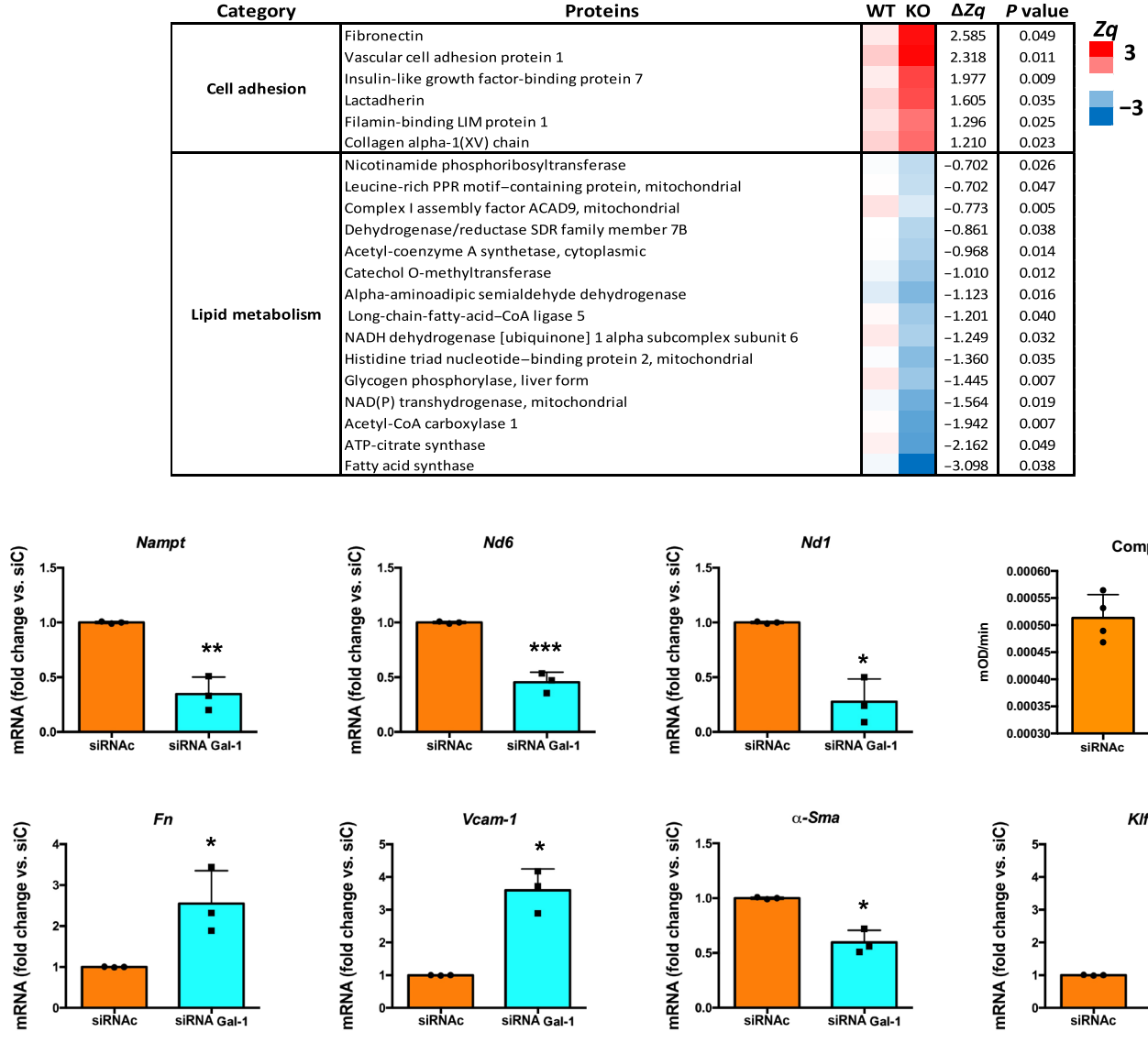

Fig. 3. Altered mitochondria and phenotypic switch in VSMCs from Gal-1–deficient mice. (**A**) Proteomic analysis of aortic homogenates from Gal-1–deficient versus WT mice. Enrichment analysis of proteins differentially expressed in aorta from WT ($n = 9$) or *Lgals1*$^{-/-}$ [knockout (KO); $n = 7$] mice showing biological processes significantly altered (FDR < 5%). The heatmap shows the average of protein abundance changes (*Zq*) in WT and KO animals in relation to the value in WT mice. Increased (red) or decreased (blue) expression is expressed according to the indicated *Zq* scale. *Zq* is measured in SD units, and Δ*Zq* is calculated as the difference between the average of *Zq* in KO and WT samples. Statistical significance of changes (*P* value) is calculated using two-tailed Student's *t* test. (**B**) Relative *Nampt*, *mt-Nd6*, and *mt-Nd1* mRNA expression normalized to *18S/Gapdh*, as well as complex 1 activity, in VSMCs transfected with Gal-1–siRNA or scrambled siRNA. (**C**) Relative *Fn1*, *Vcam-1*, α-*Sma*, and *Klf4* mRNA expression normalized to *18S/Gapdh* mRNA of VSMCs transfected with Gal-1–siRNA or scrambled siRNA for 48 hours and treated with TNF (100 ng/ml) for 24 hours. Data are means ± SEM of three independent experiments. **P* < 0.05, ***P* < 0.01, and ****P* < 0.001, Student's *t* test.

When we analyzed proteins that were significantly up-regulated in biological processes, fibronectin (Fn1) and vascular cell adhesion molecule-1 (Vcam-1) showed the highest differences between both genotypes. Consistent with the proteomic data, both *Fn1* and *Vcam1* mRNA expression were increased in Gal-1–silenced VSMCs after tumor necrosis factor (TNF) stimulation (Fig. 3C). Because Fn1 and VCAM-1 have been previously associated with a VSMC phenotype switch in atherosclerosis (*3*, *15*–*19*) and loss of VSMC contractile phenotype has been associated with altered mitochondrial biology and a metabolic shift to glycolysis (*20*), we further analyzed the impact of Gal-1 deletion in the regulation of markers associated to VSMC phenotypic modulation, such as α-SMA and KLF4 (indicating contractile and synthetic phenotypes, respectively). α-*Sma* mRNA expression was substantially down-regulated, while *Klf4* mRNA was up-regulated in Gal-1–silenced VSMCs (Fig. 3C).

To gain further insights into the role of Gal-1 in regulating mitochondrial fitness in VSMCs, we tested the effect of Gal-1 on mitochondrial genes and function. We found that Gal-1–silenced VSMCs displayed a decrease in the transcription of genes encoding mitochondrial complexes (mt-CO1 and mt-SDH) and those implicated in mitochondrial function (TFAM and PPARα) (Fig. 4A). When we analyzed cellular metabolism, we found that oxygen consumption

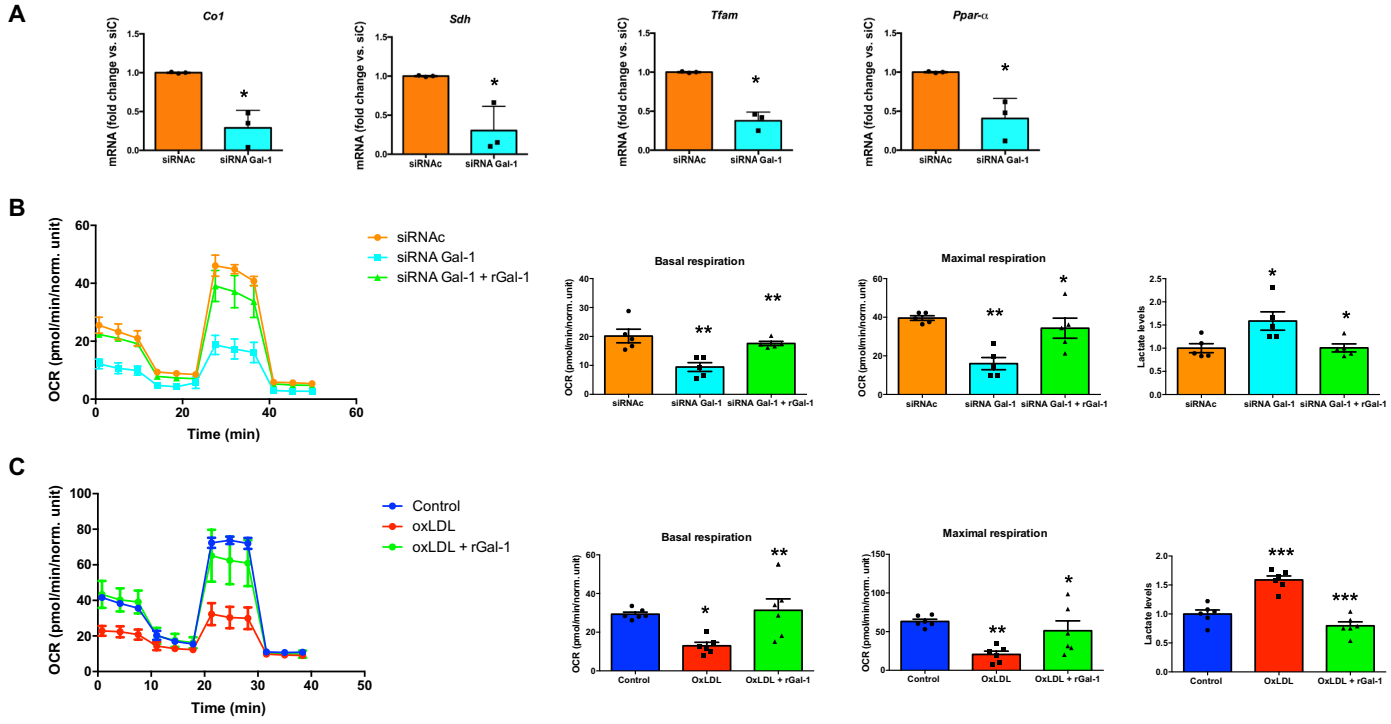

Fig. 4. Gal-1 alters mitochondrial fitness in VSMCs. (**A**) Relative *Co-1*, *Sdh*, *Tfam*, and *Ppar-α* mRNA expression normalized to *18S*/*Gapdh* in VSMCs transfected with Gal-1–siRNA or scrambled siRNA. (**B**) Graphs depicting the OCR and extracellular lactate levels in VSMCs transfected with scrambled siRNA or Gal-1–siRNA exposed or not to rGal-1 (1 μg/μl, 48 hours). (**C**) Graphs depicting the OCR and extracellular lactate levels in VSMCs incubated with oxLDL (0.1 mg/ml, 48 hours) with or without rGal-1 (1 μg/μl, 48 hours). Data are means ± SEM of five to six independent experiments. **P* < 0.05, ***P* < 0.01, and ****P* < 0.001, Student's *t* test [for (A)] and ANOVA test followed by Tukey's test [for (B) and (C)].

rate (OCR) was significantly decreased in Gal-1–silenced VSMCs (Fig. 4B). Moreover, heightened glycolysis, as measured by the extracellular lactate levels, was increased in Gal-1–silenced VSMCs (Fig. 4B). Given these findings, we then investigated whether rGal-1 could alleviate mitochondrial dysfunctionality in Gal-1–silenced VSMCs or in VSMCs incubated with oxidized LDL (oxLDL; 0.1 mg/ml for 48 hours) (Fig. 4, B and C). Of note, exposure to rGal-1 or its vehicle β-mercaptoethanol (contained in Gal-1 preparation) did not alter LDL oxidation (fig. S4). Treatment with rGal-1 (1 μg/ml) prevented both the decreased OCR and the increased extracellular lactate production, induced by Gal-1 siRNA or oxLDL (Fig. 4, B and C). Thus, Gal-1 controls vascular remodeling through mechanisms involving modulation of mitochondrial function and phenotypic switch of VSMCs.

Treatment with rGal-1 mitigates atherosclerotic plaque formation and AAA development

Given the deleterious effect of Gal-1 deletion in the stability of advanced atherosclerotic plaques, and the beneficial effect of rGal-1 on foam cell formation and VSMC mitochondrial function, we then studied the potential therapeutic effects of rGal-1 administration during the development of vascular pathology. As observed by ORO staining, in vivo supplementation with rGal-1 resulted in a 34% reduction of lesion area in the aorta as compared to administration of vehicle control (Fig. 5A). However, no differences were observed in body weights (44.1 ± 0.8 versus 43.5 ± 0.9 g, *P* = NS) or lipid content (total cholesterol = 38.6 ± 6.3 versus 43.6 ± 8.5 mM; VLDL-LDL cholesterol = 36.5 ± 6.2 versus 42.1 ± 8.4 mM, *P* = NS) between vehicle-treated and rGal-1–treated mice, respectively. Moreover, when we compared atherosclerotic lesion size in the aortic root, mice treated with rGal-1 exhibited significantly reduced plaque size compared with mice treated with vehicle control (Fig. 5B). We then measured different markers of plaque stability in both groups. No changes were observed for lesional lipid or collagen content (Fig. 5, C and E), while a reduction in necrotic core area was evident in mice treated with rGal-1 (Fig. 5D).α-SMA and calponin staining was greater in mice treated with rGal-1 compared with those treated with vehicle control (Fig. 5F and fig. S2), while CD68 staining was similar in both mouse groups (Fig. 5G).

To investigate whether the protective effects of Gal-1 in advanced atherosclerosis were also verified in other conditions involving pathological vascular remodeling, we further explored the role of this lectin in AAA. We first analyzed Gal-1 expression in human AAA tissue samples. Our findings revealed a reduction of Gal-1, along with α-SMA staining, when comparing the media layer of AAA with that of healthy aorta (Fig. 6A). Soluble Gal-1 was also decreased in AAA wall tissue-conditioned medium compared to control aortas (Fig. 6B). Further analysis of mRNA expression confirmed down-regulation of *LGALS1* and α-*SMA* mRNA expression in human AAA tissues (Fig. 6, C and D). *Lgals1* mRNA was also decreased in aortic walls obtained from elastase-induced AAA as compared with control aortas (Fig. 6E). Moreover, treatment with rGal-1 (100 μg/3 days a week) led to smaller aortic dilation and higher contractile VSMC content, as shown by α-SMA staining and calponin, compared with vehicle-treated mice (Fig. 6F and fig. S2), while no significant changes were observed in CD68 expression

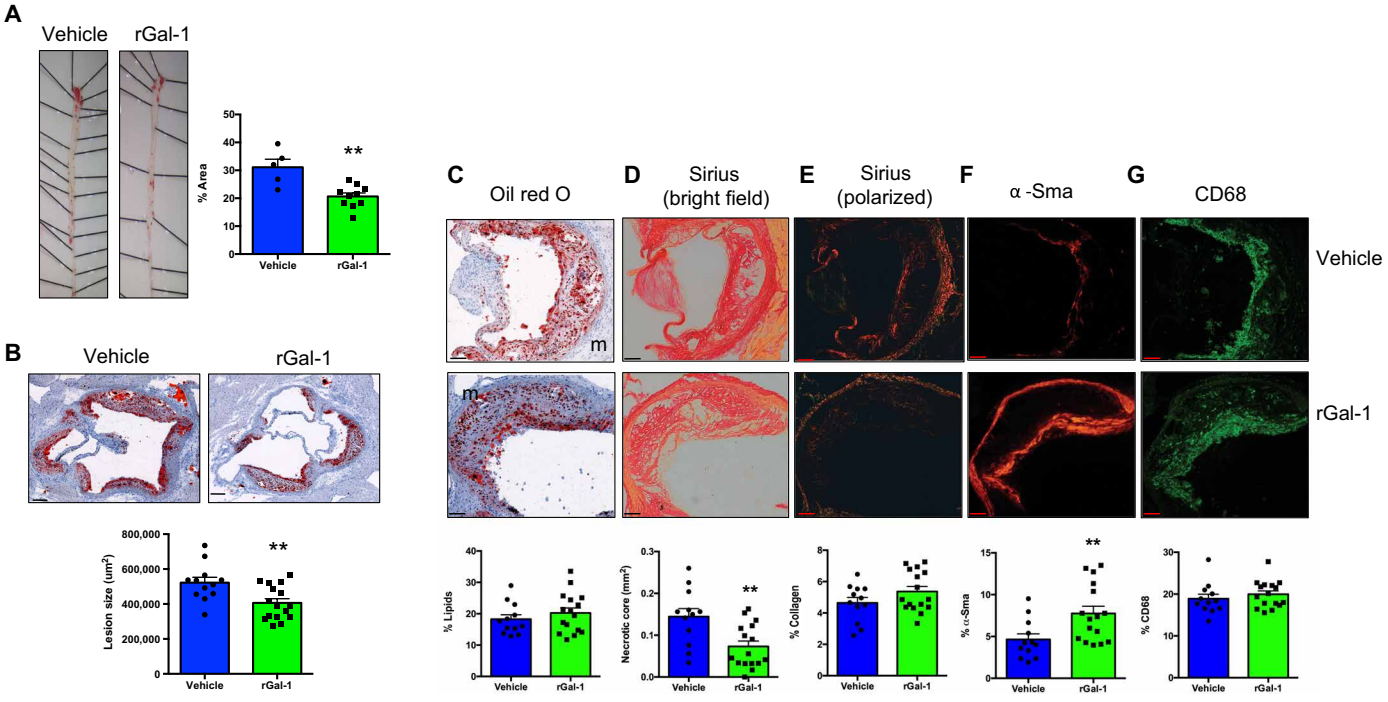

Fig. 5. Treatment with recombinant Gal-1 limits the severity of atherosclerosis and enhances atherosclerotic plaque stability in mice. (**A**) Representative ORO staining in whole aorta of saline-treated ($n = 5$) or rGal-1–treated ($n = 10$) mice at 16-week harvest after AAV-PCSK9 infection and high-fat diet. (**B**) Representative ORO/hematoxylin staining in the aortic root of WT mice treated with rGal-1 ($n = 16$) compared with saline-treated WT mice ($n = 12$) at 16-week harvest after AAV-PCSK9 infection and high-fat diet. Scale bars, 200 μm. (**C** to **G**) Representative photographs and quantification of ORO (C), Sirius red [bright field (D) and polarized (E)], α-Sma (F), and CD68 (G) staining in the aortic root of WT mice treated with rGal-1 ($n = 16$) compared with WT mice saline-treated ($n = 12$) at 16-week harvest after AAV-PCSK9 infection and high-fat diet. Scale bars, 100 μm. Values are means ± SEM. *$P < 0.05$ or **$P < 0.01$, Mann-Whitney *U* test.

(Fig. 6F). These results highlight the therapeutic value of rGal-1 supplementation in chronic pathologies involving vascular remodeling.

DISCUSSION

The dual role of Gal-1 in modulating inflammatory and vascular responses (*6*, *10*, *21*, *22*) prompted us to investigate the contribution of this lectin to pathological vascular remodeling in atherosclerosis and AAA. We demonstrated through a global loss-of-function approach that Gal-1 deficiency results in increased atherosclerotic burden and instability. Treatment with rGal-1 protein prevents development and instability of atherosclerotic plaques and AAA. Last, Gal-1 expression was down-regulated in human atherosclerotic plaques and AAA.

Expression of Gal-1 was initially observed in human coronary atherosclerotic lesions associated to intimal proliferating VSMCs (*23*) and later detected in murine atherosclerotic lesions, in both the media and intima layers (*24*). More recently, expression of this lectin was identified in endothelial cells and VSMCs in normal vessels of control mice and also in intimal VSMCs of injured vessels obtained after angioplasty in a mice carotid artery ligation model (*25*). Here, we identified high Gal-1 expression in healthy aortas, mainly composed of VSMCs, while atherosclerotic plaques and AAA showed lower expression. Although previous studies have not analyzed Gal-1 expression in human AAA tissues, it was recently reported that this lectin is significantly elevated in aortic tissues of angiotensin II–infused AAA in mice (*26*). In contrast, we have shown a decrease in Gal-1 expression in elastase-induced AAA in mice. Thus, Gal-1 expression not only varies between human and mouse AAA but also fluctuates among different AAA experimental models (*27*). It is well known that atherosclerosis and AAA progression are linked to a decrease in VSMC content and/or by loss of contractile markers of VSMCs (*15*–*18*, *28*). Thus, whether the overall decreased expression of Gal-1 in human atherosclerotic tissue or AAA is associated to a decreased content of VSMC and α-SMA expression or whether it is due to a protective effect of this lectin in pathological vascular remodeling is an intriguing question.

To evaluate the relevance of Gal-1 in advanced atherosclerosis, we used an atherosclerotic model based on pAAV/D377Y-mPCSK9 injection along with high-fat diet for 16 weeks, which increases circulating lipid levels by altering LDLr recycling and, consequently, generates lipid-rich atherosclerotic plaques (*29*). Atherosclerosis is a systemic diffuse disease, which affects different territories, supporting the importance of analyzing the global atherosclerotic burden (*30*). We measured the atherosclerotic plaques along the whole aorta by enface analysis, showing a higher atherosclerotic burden in Gal-1–deficient mice as compared to WT mice. Unexpectedly, *Lgals1*$^{-/-}$ mice displayed higher systemic cholesterol levels under hyperlipidemic conditions. Thus, we studied whether main receptors involved in liver lipoprotein clearance could be altered under our experimental conditions; however, no differences were found on *LDLr* or *VLDLr* mRNA expression. Furthermore, nontargeted proteomic analysis of liver samples of *Lgals1*$^{-/-}$ and WT mice showed no major changes in lipid metabolic processes. Thus, further analysis should be performed to evaluate the potential role of Gal-1 in liver VLDL assembly and secretion under hyperlipidemic conditions. Last, we also found

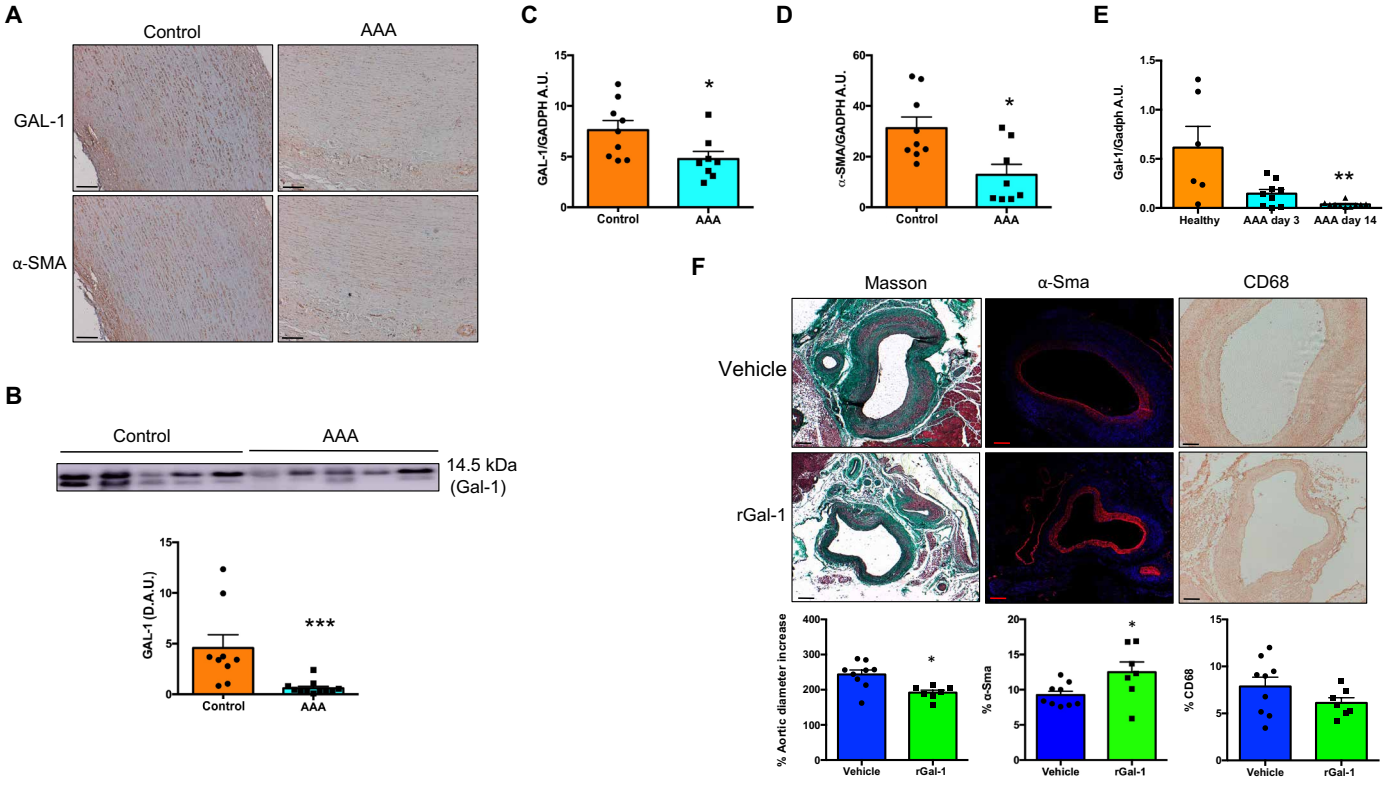

Fig. 6. Treatment with recombinant Gal-1 mitigates AAA development. (**A**) Representative immunohistochemistry of GAL-1 expression in the wall of human AAA patients and control aorta. Scale bar, 100 μm. (**B**) GAL-1 expression was determined by Western blot in conditioned medium from the AAA wall ($n = 11$) and healthy aortic tissue ($n = 9$). (**C** and **D**) Determination of *LGALS1 mRNA* (C) and α-*SMA* (D) mRNA in the wall of human AAA tissues ($n = 8$) versus healthy human control aortic samples ($n = 9$). (**E**) Determination of *Lgals1* mRNA in the wall of elastase-induced AAA at day 3 ($n = 8$) and at day 14 ($n = 10$) versus healthy aortic samples ($n = 6$). (**F**) Representative Masson's trichrome staining and quantification of the increment of aortic diameter at 14 days after perfusion of elastase in saline-treated ($n = 9$) and Gal-1–treated (rGal-1, $n = 7$) mice. Scale bars, 200 μm. Representative α-Sma and CD68 staining and quantification at 14 days after perfusion of elastase in saline-treated ($n = 9$) and Gal-1–treated (rGal-1, $n = 7$) mice. Scale bars, 200 μm. Values are means ± SEM. *$P < 0.05$, **$P < 0.01$, and ***$P < 0.001$, Mann-Whitney *U* test.

an increase in maximal lesion size in Gal-1–deficient mice compared to WT mice in the aortic root, in agreement with the enface analysis on the whole aorta. Moreover, we found a higher content of lipids inside atherosclerotic plaques in Gal-1–deficient mice, while we could not find significant changes in the necrotic core area and collagen content. We also observed a greater uptake of oxLDL by peritoneal macrophages from *Lgals1*$^{-/-}$ versus WT mice, which favored LDL retention inside the arterial wall; this effect was prevented by exposure to rGal-1, suggesting an important role of Gal-1 in limiting foam cell formation. Last, the percentage of α-SMA and calponin staining was decreased in Gal-1–deficient mice, while no changes in CD68 expression were detected. Collectively, these data support a protective role of Gal-1 in atherosclerosis by modulating critical determinants of plaque progression and instability.

We then performed an unbiased proteomic analysis of whole aorta homogenates to elucidate possible mechanisms associated with Gal-1 effects. We found that, among biological pathways and cellular processes significantly enriched by Database for Annotation, Visualization and Integrated Discovery (DAVID) analysis in the aorta of *Lgals1*$^{-/-}$ mice, mitochondrial proteins were clearly down-regulated. A decline in the expression of mitochondrial components and/or factors involved in mitochondrial activity was also observed after Gal-1 silencing in VSMCs. Impaired mitochondrial respiration and reduced oxidative phosphorylation in VSMCs have been linked to atherosclerosis progression (*31*–*33*). In addition, we have recently observed that VSMCs from patients with aneurysm also display dysfunctional mitochondria associated to a synthetic phenotypic switch (*34*). In this regard, lineage-tracing studies revealed that the progeny of VSMCs has a remarkable plasticity in the vascular wall and can assume a wide variety of phenotypes during vascular remodeling, including loss of contractile markers, while adopting alternative phenotypes characteristic of foam cells, osteochondrocytes, or myofibroblasts, among others (*17*, *35*–*39*). In this regard, aortic proteomics analysis also identified a clear up-regulation of Fn and VCAM-1, which are commonly associated with phenotypic modulation of VSMCs, being Fn linked with a profibrotic state and VCAM-1 expression connected with a proinflammatory VSMC profile (*15*–*18*). In agreement, we found that Gal-1 silencing resulted in enhanced *Fn1* and *Vcam-1* mRNA expression in TNF-stimulated VSMCs in vitro. Our proteomics data in whole aorta, and the decrease in α-SMA expression in atherosclerotic plaques of *Lgals1*$^{-/-}$ mice, led us to examine whether Gal-1 silencing has a direct role on VSMC phenotypic switch. We also observed increased KLF4 and decreased α-SMA expression in Gal-1–silenced VSMCs. Similarly, Gal-1 knockdown in VSMCs incubated with platelet-derived growth factor (PDGF)–BB decreased α-SMA expression (*40*), while Gal-1 induced α-SMA expression in fibroblasts (*41*, *42*). In this regard, loss of VSMC contractile phenotype has been associated with a metabolic

shift to glycolysis and altered mitochondrial fitness (*20*, *32*). Synthetic VSMCs demonstrated an increased glycolytic flux, with a decrease in glucose oxidation (*43*). We found that Gal-1–silenced VSMCs showed decreased OCR (an indicator of mitochondrial oxidative phosphorylation) but displayed increased lactate production. rGal-1 reversed the increased OCR and decreased lactate induced by Gal-1 siRNA or oxLDL in VSMCs. In this regard, it was previously described that, in a lactate-enriched microenvironment, VSMCs acquire a synthetic phenotype (*44*). Thus, altered lactate production via Gal-1 modulation might contribute to a loop of VSMC phenotypic switch. Our data suggest a central role of Gal-1 in mitochondrial functionality and phenotypic switch of VSMCs during vascular remodeling.

Currently, atherosclerosis is mostly treated with drugs that modulate CV risk factors, including statins to prevent CV risk. However, residual CV risk persists and new approaches mainly focused on anti-inflammatory agents are being tested (*45*, *46*). In this regard, previous studies demonstrated the protective role of rGal-1 treatment in the resolution of acute and chronic inflammatory conditions (*47*), including AMI (*11*), autoimmune neuroinflammation (*48*), inflammatory bowel diseases (*49*), and diabetes (*50*, *51*). In this study, we investigated the role of Gal-1 as a novel therapeutic strategy in two different chronic vascular diseases, such as atherosclerosis and AAA. In advanced atherosclerosis, treatment with rGal-1 decreased atherosclerotic burden, independently of plasma lipid levels. Moreover, Gal-1 administration reduced maximal lesion size and necrotic core extension at the aortic root, along with increased α-SMA staining, but did not alter CD68 expression. Similarly, in AAA, rGal-1 supplementation was associated with prevention of α-SMA loss but did not modify the frequency of CD68 expression, suggesting no major changes in the control of macrophage infiltration in this pathologic setting. In contrast, it has been recently shown that Gal-1 deficiency reduced the incidence and severity of angiotensin-induced AAA by decreasing vascular inflammation (*26*). In that particular study, the authors suggested that the absence of oxidized Gal-1 associated to Gal-1 deletion could be responsible for the protective effect in AAA. The discrepancies with our study could be related to differences between approaches (Gal-1 deletion versus treatment with rGal-1), reflecting the effects of the endogenous versus exogenous lectin, and between experimental models (*27*). Our data suggest that treatment with rGal-1 is vasculoprotective in both atherosclerosis and AAA through mechanisms involving modulation of foam cell formation, as well as mitochondrial metabolic fitness and preservation of VSMC contractile phenotype. Because of the increasing importance of the diverse VSMC phenotypes in vascular remodeling (*15*–*18*, *37*), molecular targets that interfere with the modulation of VSMC fate could be envisioned as alternative approaches to treat chronic vascular pathologies (*52*). We and others have previously shown that different members of the galectin family, including Gal-3, can also modulate physiologic and pathologic vascular remodeling (*53*–*55*), highlighting the involvement of a coordinated galectin-glycan network in controlling chronic vascular processes.

Some limitations of our study should be discussed. The experimental model of atherosclerosis used in this study (AAV-PCSK9) develops extensive lesions in the aortic root, the aorta,

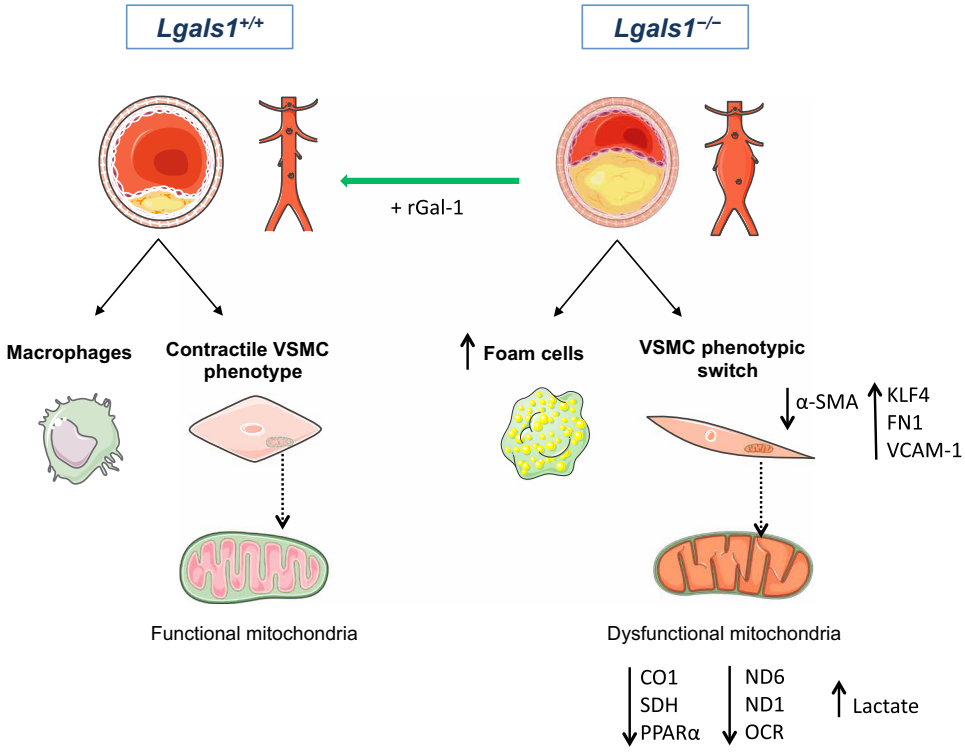

Fig. 7. Proposed model: Role of Gal-1 in pathological vascular remodeling. The development of atherosclerosis and AAA is associated with down-regulation of Gal-1 expression. Treatment with rGal-1 attenuated both PCSK9-AAV–induced atherosclerosis and elastase-induced AAA. The mechanisms underlying these protective effects involve modulation of foam cell formation and control of mitochondria functionality in VSMCs, preventing the loss of contractile VSMC phenotype.

and its principal branches, similar to most common models of atherosclerosis (ApoE and Ldlr ko mice); however, they fail to develop atherosclerosis in the coronary arteries. Moreover, plaque rupture and thrombotic occlusion rarely occur in the coronary arteries in these models. Thus, we only assessed the effect of Gal-1 in plaque progression and instability using indirect markers, such as lipid content in the plaques, the presence of a necrotic core, and the frequency of contractile VSMCs. To enhance the translational application of our findings, new models that better resemble human conditions should be tested. In this respect, transverse aortic constriction performed in *ApoE*$^{-/-}$ mice can lead to coronary plaque formation, progression, and myocardial events (*56*).

Our results suggest that Gal-1 affects both macrophage and VSMC functionality and metabolism. Although we did not observe changes in CD68 expression, we cannot rule out a possible anti-inflammatory effect of Gal-1 in macrophage number as CD68 is not a specific marker of myeloid cells (*57*). CD68 and other markers that are frequently used to identify macrophages may also be expressed in VSMCs (*53*, *58*). Thus, further studies targeting Gal-1 specifically in hematopoietic cells and/or VSMCs would contribute to better define the role of this lectin in regulating atherosclerotic lesions in vivo.

In summary, our findings support a broad protective role of Gal-1 in pathological vascular disorders through mechanisms involving modulation of lipid uptake by macrophages along with alterations in mitochondrial function and phenotypic switch of VSMCs (Fig. 7). Treatment with rGal-1 prevented both atherosclerosis and AAA in mice, highlighting the therapeutic potential of this lectin in attenuating the severity of chronic pathologic vascular remodeling. Last, decreased expression of Gal-1 in advanced human atherosclerosis and AAA underlines the clinical relevance of our findings.

MATERIALS AND METHODS

Human tissues

Aortas were collected from deceased organ donors under the authorization of the French Biomedicine Agency (PFS 09-007, BBMRI network, BB-0033-00029). Ethical committee advice and patient written informed consent were obtained before participation (RESAA and AMETHYST studies, CPP Paris-Cochin 2095, 1930, and 1931, INSERM Institutional Review Board, IRB0000388). All human studies conformed to the principles outlined in the Declaration of Helsinki.

After macroscopic examination, the aortas were classified according to Stary classification (*59*) and the Virmani word list (*4*) into control aortas (devoid of atheromatous lesions) and aortas with atherosclerotic plaques. In addition, AAA walls were collected from patients who were undergoing surgical repair of AAA. A small portion of tissue from each sample was fixed in 3.7% paraformaldehyde for classical histology and immunohistochemistry assessments. In atherosclerotic aortas, the adventitia and media were carefully removed, and the dissected intimal lesion was processed separately, while in AAA, the adventitia was removed and the media layer was further processed. Atherosclerotic plaques, as well as control aortas and AAA tissues, were either incubated in culture medium to obtain tissue-conditioned medium or placed in liquid N_2 for later RNA or protein extraction. For tissue-conditioned medium, samples were cut into small pieces (5 mm^2) and incubated in RPMI 1640 medium without fetal bovine serum (FBS) for 24 hours at 37°C (6 ml/g of wet tissue). The tissue-conditioned medium was collected after centrifugation at 3000*g* for 10 min at 20°C and frozen at −80°C.

Experimental models

Gal-1–deficient mice (*Lgals1*$^{-/-}$; C57BL6/J) were originally provided by F. Poirier (Jacques Monod, Paris, France). The corresponding WT control mice (C57BL6/J) were purchased from The Jackson Laboratory (Bar Harbor, USA). No differences in size and weight were detected between WT and *Lgals1*$^{-/-}$ mice. All animals were housed in isolation rooms at the Animal Facilities of the Institute of IIS-Fundación Jiménez Díaz. The Ethics Review Board of the Institute of IIS-Fundación Jiménez Díaz approved all animal procedures, and the project was authorized by the IIS-FJD-Universidad Autónoma de Madrid (CEI 59-1036-A061) and by the Spanish Authority governing animal experimentation, the Comunidad Autónoma de Madrid (registered approval letter 10/008932.9/15). All animal procedures were performed in accordance with the guidelines of Directive 2010/63/EU of the European Parliament on the protection of animals used for scientific purposes.

The experimental model of atherosclerosis was induced in a 10-week-old male as described (*13*). Mice were maintained on normal diet before pAAV/D377Y-mPCSK9 injection (a gift of J. Bentzon, Aarhus University). The same viral preparation was aliquoted before storage and used for all studies. C57BL6/J WT and *Lgals1*$^{-/-}$ mice were given retro-orbital injections of 10^{11} vector genome copies of pAAV/D377Y-mPCSK9. Immediately following the AAV-PCSK9 injection, mice were switched to a high-fat diet (TD88137, Envigo) for 16 weeks. Two experimental approaches were performed. First, we analyzed the role of endogenous Gal-1 by comparing WT (n = 10) and *Lgals1*$^{-/-}$ (n = 12) mice. An additional group of WT (n = 5) and *Lgals1*$^{-/-}$ (n = 5) mice was subjected to similar conditions and used for enface analysis. Second, we tested the therapeutic effects of exogenous Gal-1 in WT mice treated with rGal-1 (100 μg/3 days a week, n = 16) compared to vehicle/saline (n = 12) during 16 weeks of high-fat diet. rGal-1 was obtained and purified as described (*60*) and diluted in PBS containing β-mercaptoethanol (0.3 μl/ml). Dose of rGal-1 was chosen on the basis of our previous studies (*48*, *49*). All mice were maintained under barrier conditions. Water and western diet were available ad libitum. At the end of the study, 16-hour fasted mice were anesthetized [ketamine (100 mg/kg) and xylazine (15 mg/kg)], saline-perfused, and euthanized. Blood samples were collected for biochemistry. Serum total cholesterol and VLDL/LDL cholesterol were measured enzymatically using commercial kits adapted for a COBAS 6000 autoanalyzer (Roche Diagnostics).

For experimental AAA, mice (C57BL6/J, 12 weeks old) were anaesthetized using 2% isoflurane, and a horizontal laparotomy was performed. Using a surgical stereomicroscope, the abdominal aorta was separated from the level of the left renal vein to the bifurcation and temporarily ligated between the renal and iliac arteries. An aortotomy was created with a 30-gauge needle, and the aorta was exsanguinated. A PE-26 polyethylene tube was introduced through the aortotomy, and the aorta was infused for 5 min at 100 mm Hg with either saline buffer (control) or type 1 porcine pancreatic elastase (specific activity, 6 U/mg protein; E1250, Sigma Chemical). The aortotomy was then repaired, the ligation was eliminated, and the restoration of blood flow was visually confirmed. Incisions were closed, and mice were housed under standard conditions. Experimental groups included elastase-infused WT mice treated with vehicle/saline (n = 9) or with rGal-1 (100 μg/3 days a week, n = 7). On day 14 after surgery, all mice were anaesthetized with a mixture of ketamine/xylazine (100 and 10 mg/kg body weight, respectively) and euthanized

by cervical dislocation. External pre-perfusion and 14-day post-perfusion aortic diameters were measured to a resolution of 0.01 mm with a calibrated ocular grid while mice were under anesthesia and physiological blood pressure. Aortic diameter expansion of ≥100% compared with that observed before perfusion defined AAA. Aortic tissue samples were obtained for histological analysis. An additional cohort of elastase-infused WT mice ($n = 8$ at day 3 and $n = 10$ at day 14, after elastase perfusion) and untreated healthy WT mice ($n = 6$) were subjected to mRNA isolation from aortic tissues.

Enface analysis of aorta

Atherosclerotic burden was quantified by enface analysis of the whole aorta. For enface preparations, the aorta was opened longitudinally from the heart to the iliac arteries while still attached to the heart and major branching arteries in the body. The aorta (from the heart to the iliac bifurcation) was then removed and pinned out on a white wax surface in a dissecting pan, using stainless steel pins 0.2 mm in diameter. After overnight fixation with 4% paraformaldehyde and a rinse in phosphate-buffered saline (PBS), the aortas were immersed for 1 hour in a filtered solution containing 0.2% ORO and unstained in 80% ethanol. The ORO-stained aortas were photographed and used for quantification of atherosclerotic lesions.

Morphometric analysis

Hearts containing aortic roots were carefully dissected and frozen in optimal cutting temperature (OCT) compound. Aortic roots were sectioned at 5 μm thickness beginning proximally at the first evidence of the aortic valves at their attachment site of aorta. Sections were treated with ORO/hematoxylin for lipid staining at 100-μm intervals from 0 to 900 μM distal to the proximal site. Maximal lesion area was calculated for each mouse by averaging the values for three sections. The individual maximal lesion areas were further averaged to determine the maximal lesion area for each mouse group. Lipid content was defined as the percentage of ORO staining area to total plaque area. Picrosirius red staining was performed for analysis of collagen content by measuring birefringence to plane-polarized light. Necrotic core was analyzed in the bright-field sections obtained after picrosirius red by delimitating the acellular areas with cholesterol clefts.

For AAA lesions, aortic tissue cross sections (3 to 4 μm) were stained with Masson's trichrome and then evaluated (*53*). Changes in aortic diameter were calculated as percentage of dilation over baseline at day 14.

Immunohistochemistry

Primary antibodies were anti–Gal-1 (AF1152, R&D Systems), CD68 (Ab53444, Abcam), and α-SMA (clone 1A4, Sigma-Aldrich). Rabbit anti-goat horseradish peroxidase (HRP), donkey anti-rat HRP (The Jackson Laboratory), and Alexa Fluor 488 donkey anti-rat (Invitrogen) were used as secondary antibodies. HRP was then added, and sections were stained with 3,3′-diaminobenzidine (DAB) substrate-chromogen (DAKO) and counterstained with hematoxylin. Computer-assisted morphometric analysis was performed with Image-Pro Plus software (version 1.0 for Windows). The threshold setting for area measurement was equal for all images. Samples from each animal were examined in a blinded manner. Results were expressed as % positive area versus total area (CD68 and α-SMA).

Proteomic analysis

Protein extraction

Samples from liver and aorta from WT and *Lgals1*$^{-/-}$ mice were processed for proteomic analysis. Protein extracts were obtained by tissue homogenization with ceramic beads (MagNaLyser Green Beads apparatus, Roche, Germany) in extraction buffer [100 mM tris-HCl (pH 6.8) and 2% SDS]. Supernatants were collected, and protein concentration was measured by RC/DC Protein Assay (Bio-Rad). Protein extracts were stored at −80°C for further analysis.

Protein digestion

Protein extracts (250 μg) were subjected to filter-aided digestion (Nanosep Centrifugal Devices with Omega Membrane-30K, PALL) according to the manufacturer's instructions. Briefly, cysteine residues were blocked with 50 mM iodoacetamide buffer and proteins were digested with trypsin (1:40 trypsin/protein; Promega) in 100 mM ammonium bicarbonate (pH 8.8) overnight at 37°C. The resulting peptides were desalted with Oasis cartridges (Waters Corporation, Milford, MA, USA) following the manufacturer's instructions, dried with SpeedVac, and stored at −20°C.

TMT labeling

Peptides were subjected to two 9-plex multiplexed isobaric labeling experiments (eight WT and eight *Lgals1*$^{-/-}$ mice) in the case of liver samples and to two 8-plex multiplexed isobaric labeling experiments (nine WT and seven *Lgals1*$^{-/-}$ mice) in the case of aorta samples, using TMT reagents (Thermo Fisher Scientific) and following the manufacturer's instructions. In each TMT experiment, one channel was reserved for a reference internal standard sample created by pooling control samples. Labeled peptides were desalted with Oasis cartridges (Waters Corporation, Milford, MA, USA), vacuum-dried, and stored at −20°C for further mass spectrometry (MS) analysis.

LC-MS analysis

Labeled peptide samples were analyzed using an Ultimate 3000 HPLC system (Thermo Fisher Scientific) coupled via a nanoelectrospray ion source (Thermo Fisher Scientific, Bremen, Germany) to a Q Exactive HF mass spectrometer (Thermo Fisher Scientific). C18-based reversed-phase separation was used with PepMap 100 C18 5UM 0.3x5MM as trapping column (Thermo Fisher Scientific) and a 50-cm analytical column (EASY-Column, Thermo Fisher Scientific). Peptides were loaded in buffer A [0.1% formic acid in water (v/v)] and eluted with a 338-min linear gradient of buffer B [100% acetonitrile and 0.1% formic acid (v/v)] at 200 nl/min. Mass spectra were acquired in a data-dependent manner, with an automatic switch between MS and MS/MS using a top-15 method. MS spectra were acquired in an Orbitrap analyzer with a mass range of 400 to 1500 m/z (mass/charge ratio) and 70,000-pixel resolution. HCD fragmentation was performed at 30 of normalized collision energy, and MS/MS spectra were analyzed at 60,000-pixel resolution in the Orbitrap.

Protein identification

For peptide identification, MS/MS spectra were searched with the SEQUEST HT algorithm implemented in Proteome Discoverer 2.1 (Thermo Fisher Scientific) against a UniProt database composed of mouse protein sequences (July 2020), using trypsin digestion with a maximum of two missed cleavages, using Cys carbamidomethylation (57.021464 Da) and TMT labeling at the N-terminal end as fixed modifications and Lys (229.162932 Da) and Met oxidation (15.994915) as dynamic modifications. Precursor mass tolerance was set at 800 parts per million (ppm), and fragment mass tolerance was set at 0.03 Da; precursor charge range was set to 2 to 4. Results were analyzed using the probability ratio method (*61*), and the FDR was

calculated based on the search of results against the corresponding decoy database using a refined method with an additional filter for precursor mass tolerance of 15 ppm (*62*). One percent FDR was used as criterion for peptide identification.

Protein quantification and statistical analysis

Protein quantification and statistical analysis were performed using the models previously developed in our laboratory (*63*–*65*) with the SanXoT software package (*66*). Quantitative information was extracted from the MS/MS spectra of TMT-labeled peptides. Peptide quantification was analyzed using the Weighted Spectrum, Peptide and Protein model, which uses raw quantifications as input data and computes the protein $\log_2$ fold changes for each individual with respect to the value of the reference internal standard sample. In this model, protein $\log_2$ ratios are expressed as standardized variables in units of SD according to their estimated variances (*Zq* values). For functional analysis, proteins were annotated using DAVID (*67*). MS proteomics data were deposited at the ProteomeXchange Consortium (*68*) via the PRIDE partner repository with the dataset identifier PXD024637.

In vitro experiments in VSMCs and macrophages

Mouse VSMCs were obtained directly from primary culture of aorta tissue of WT mice. The aorta was carefully removed from the iliac arteries to the heart and immersed in PBS. To remove undesirable leftovers, aortas were cleansed physically, cut into small pieces, and enzymatically treated with 4 mg of collagenase per aorta (Sigma Life Science) in dulbecco´s minimum esssential medium (DMEM)–F12 medium (Thermo Fisher Scientific) plus 20% FBS and were further seeded in p60 plaques and incubated at 37°C for 5 days. Cells were harvested for passaging at 2- to 3-day intervals and used between the second and seventh passages. For experiments except those of seahorse, cells were FBS-depleted for 24 hours and, in some cases, stimulated for 24 hours with TNF (100 ng/ml) before cells were pelleted and resuspended for RNA analysis. LDLs from a pool of serum of healthy donors were obtained by ultracentrifugation and oxidized by incubation with 5 mM $CuSO_4$ for 18 hours at 37°C.

Peritoneal macrophages were collected from *WT* or *Lgals1*$^{-/-}$ mice by peritoneal lavage 4 days after intraperitoneal injection of 3% (w/v) thioglycolate. Cells were cultured for 24 hours in RPMI 1640 supplemented with 10% FBS, L-glutamine, and antibiotics. Then, cells were incubated with Dil-oxidized LDL (10 μg/ml) for 4 hours. Cells were fixed in 4% paraformaldehyde for 15 min and stained with 4′,6-diamidino-2-phenylindole (DAPI). Percentage of foam cells was analyzed in 5 to 10 random fields per cell culture as described (*69*).

siRNA-mediated knockdown assays

siRNA specific for mouse Gal-1 was obtained from Santa Cruz Biotechnology (sc-37259). Transfection of siRNA was performed using Lipofectamine as described (*70*). Experiments were also performed with a negative control available from Ambion (AM4636).

Real-time PCR

Human atherosclerotic or AAA tissues, as well as aortic wall tissues from healthy human controls, and mouse aortic and liver homogenates were snap-frozen in liquid nitrogen; homogenates (0.2 g) were resuspended in TRIzol buffer (Life Technologies); and total RNA was purified. Similarly, lysates from VSMCs were resuspended in TRIzol, and total RNA was purified. Duplicate samples were quantified by determining absorbance at 260 nm, and real-time PCR was performed as described (*53*). The expression of target genes was normalized to housekeeping transcript [18*S*/glyceraldehyde-3-phosphate dehydrogenase (GAPDH)]. The following PCR primers for human [*LGALS1*, 5′-CTGCAACACTTCCAGGCTGG-3′ (reverse) and 5′-CCTGGAGAGTGCCTTCGAGTG-3′ (forward); *ACTA2*, 5′-GCTCAGCAGTAGTAACGAAGGA-3′ (reverse) and 5′-CTATGAGGGCTATGCCTTGCC-3′ (forward)] and for mouse [*Lgals1*, 5′-TCAGCCTGGTCAAAGGTGAT-3′ (reverse) and 5′-TGAACCTGGGAAAAGACAGC-3′ (forward); *Acta2*, 5′-TTAGCATAGAGATCCTTCCTG-3′ (reverse) and 5′-CATCTTTCATTGGGATGGAG-3′ (forward); mt-Nd6, 5′-GGTTAGCATTAAAGCCTTCACCT-3′ (reverse) and 5′-CATCAACCAATCTCCCAAACCAT-3′ (forward); *Namp*, 5′-TGCCGTGAAAAGAAGACAGA-3′ (reverse) and 5′-ACTTCTTTGGCCTCCTGGAT-3′ (forward); *mt-Co1*, 5′-CTCGCCTAATTTATTCCACTTCA-3′ (reverse) and 5′-GGGGCTAGGGGTAGGGTTAT-3′ (forward); *mt-Nd1*, 5′-CTAGCAGAAACAAACCGGGC-3′ (reverse) and 5′-CCGGCTGCGTATTCTACGTT-3′ (forward); *Tfam*, 5′-CAGGAGGCAAAGGATGATTC-3′ (reverse) and 5′-CCAAGACTTCATTTCATTGTCG-3′ (forward); *Sdh*, 5′-CTTGAATCCCTGCTCTGTGG-3′ (reverse) and 5′-AAAGCTGAGAGTGCCAAGAG-3′ (forward); *Ppar-α*, 5′-TCGAGGAAGGCACTACACCT-3′ (reverse) and 5′-TCTTCCCAAAGCTCCTTCAA-3′ (forward); *Gapdh*, 5′-GGCATGGACTGTGGTCATGAG-3′ (reverse) and 5′-TGCACCACCAACTGCTTAGC-3′ (forward)] and TaqMan probes (*18s*: 4310875; *Klf4*: Mm00516104_m1; *Fn1*: Mm01256744_m1; *Vldlr*: Mm00443298_m1; *Ldlr*: Mm00440169_m1; *Vcam-1*: Mm01320970_m1) were purchased from Applied Biosystems and optimized according to the manufacturer's protocol.

Western blot

For tissue-conditioned medium, the procedure was normalized by incubating each gram of wet tissue in 6 ml of RPMI 1640 alone (without FBS) and equal amounts of proteins (20 μg) were subjected to SDS–polyacrylamide gel electrophoresis. Polyvinylidene difluoride membranes were incubated with an anti–Gal-1 monoclonal antibody (R&D Systems) and processed as previously described (*70*). Membranes were subjected to densitometry, and values were normalized against Ponceau Red S staining.

Mitochondrial functional studies

Complex I activity

Complex I activity was measured using the Complex I Enzyme Activity Microplate Assay Kit (ab109721, Abcam) following the manufacturer's instructions. Cells were pelleted after siRNA transfection, and whole-cell lysates were analyzed.

Extracellular flux analysis

OCRs were measured in XF-96 Extracellular Flux Analyzers (Seahorse Bioscience) as described (*71*) in mouse aortic VSMCs. Briefly, mouse aortic VSMCs were seeded in nonbuffered DMEM containing either 25 mM glucose or 1 mM $CaCl_2$. Three measurements were obtained under basal conditions and on addition of oligomycin (1 mM), fluoro carbonyl cyanide phenylhydrazone (1.5 mM), and rotenone (100 nM) + antimycin A (1 mM).

Extracellular L-lactate determination

Extracellular lactate determination was performed in conditioned medium (20 μl) after 48 hours for both siRNA-transfected cells and cells treated with oxLDL with single-use reagent strips for Accutrend Plus Lactate Pro (Roche), based on an enzymatic spectrophotometry system by lactate oxidase layer. OCR measurements and L-lactate were normalized to total protein cell extracts.

Statistical analysis

Results are expressed as means ± SE. For analysis of data from human samples or from the experimental models, groups were compared with the Mann-Whitney test. In vitro experiments were replicated at least three times and analyzed by Student's *t* test or the analysis of variance (ANOVA) test followed by Tukey's as appropriate. Statistics were performed using SPSS software (23.0; SPSS Inc., Chicago). Significance was defined as $P < 0.05$ (two-tailed).

SUPPLEMENTARY MATERIALS

Supplementary material for this article is available at https://science.org/doi/10.1126/sciadv.abm7322

View/request a protocol for this paper from *Bio-protocol*.

REFERENCES AND NOTES

1. G. A. Roth, G. A. Mensah, C. O. Johnson, G. Addolorato, E. Ammirati, L. M. Baddour, N. C. Barengo, A. Z. Beaton, E. J. Benjamin, C. P. Benziger, A. Bonny, M. Brauer, M. Brodmann, T. J. Cahill, J. Carapetis, A. L. Catapano, S. S. Chugh, L. T. Cooper, J. Coresh, M. Criqui, N. DeCleene, K. A. Eagle, S. Emmons-Bell, V. L. Feigin, J. Fernández-Solà, G. Fowkes, E. Gakidou, S. M. Grundy, F. J. He, G. Howard, F. Hu, L. Inker, G. Karthikeyan, N. Kassebaum, W. Koroshetz, C. Lavie, D. Lloyd-Jones, H. S. Lu, A. Mirijello, A. M. Temesgen, A. Mokdad, A. E. Moran, P. Muntner, J. Narula, B. Neal, M. Ntsekhe, G. Moraes de Oliveira, C. Otto, M. Owolabi, M. Pratt, S. Rajagopalan, M. Reitsma, A. L. P. Ribeiro, N. Rigotti, A. Rodgers, C. Sable, S. Shakil, K. Sliwa-Hahnle, B. Stark, J. Sundström, P. Timpel, I. M. Tleyjeh, M. Valgimigli, T. Vos, P. K. Whelton, M. Yacoub, L. Zuhlke, C. Murray, V. Fuster; GBD-NHLBI-JACC Global Burden of Cardiovascular Diseases Writing Group, Global burden of cardiovascular diseases and risk factors, 1990–2019: Update From the GBD 2019 study. *J. Am. Coll. Cardiol.* **76**, 2982–3021 (2020).
2. P. Libby, J. E. Buring, L. Badimon, G. K. Hansson, J. Deanfield, M. S. Bittencourt, L. Tokgözoğlu, E. F. Lewis, Atherosclerosis. *Nat. Rev. Dis. Primers* **5**, 56 (2019).
3. C. Yap, A. Mieremet, C. J. M. de Vries, D. Micha, V. de Waard, Six shades of vascular smooth muscle cells illuminated by KLF4 (Krüppel-like factor 4). *Arterioscler. Thromb. Vasc. Biol.* **41**, 2693–2707 (2021).
4. J. F. Bentzon, F. Otsuka, R. Virmani, E. Falk, Mechanisms of plaque formation and rupture. *Circ. Res.* **114**, 1852–1866 (2014).
5. M. Torres-Fonseca, M. Galan, D. Martinez-Lopez, L. Cañes, R. Roldan-Montero, J. Alonso, T. Reyero-Postigo, M. Orriols, N. Mendez-Barbero, M. Sirvent, L. M. Blanco-Colio, J. Martínez, J. L. Martin-Ventura, C. Rodríguez, Pathophisiology of abdominal aortic aneurysm: Biomarkers and novel therapeutic targets. *Clin. Investig. Arterioscler.* **31**, 166–177 (2019).
6. G. A. Rabinovich, D. O. Croci, Regulatory circuits mediated by lectin-glycan interactions in autoimmunity and cancer. *Immunity* **36**, 322–335 (2012).
7. M. A. Toscano, V. C. Martínez Allo, A. M. Cutine, G. A. Rabinovich, K. V. Mariño, Untangling galectin-driven regulatory circuits in autoimmune inflammation. *Trends Mol. Med.* **24**, 348–363 (2018).
8. F. T. Liu, R. Y. Yang, D. K. Hsu, Galectins in acute and chronic inflammation. *Ann. N. Y. Acad. Sci.* **1253**, 80–91 (2012).
9. D. Cooper, A. J. Iqbal, B. R. Gittens, C. Cervone, M. Perretti, The effect of galectins on leukocyte trafficking in inflammation: Sweet or sour? *Ann. N. Y. Acad. Sci.* **1253**, 181–192 (2012).
10. A. M. Cutine, C. A. Bach, F. Veigas, J. P. Merlo, L. Laporte, M. N. Manselle Cocco, M. Massaro, N. Sarbia, R. M. Perrotta, Y. D. Mahmoud, G. A. Rabinovich, Tissue-specific control of galectin-1-driven circuits during inflammatory responses. *Glycobiology* **31**, 891–907 (2021).
11. I. M. Seropian, G. E. González, S. M. Maller, D. H. Berrocal, A. Abbate, G. A. Rabinovich, Galectin-1 as an emerging mediator of cardiovascular inflammation: Mechanisms and therapeutic opportunities. *Mediators Inflamm.* **2018**, 8696543 (2018).
12. I. M. Seropian, J. P. Cerliani, S. Toldo, B. W. Van Tassell, J. M. Ilarregui, G. E. González, M. Matoso, F. N. Salloum, R. Melchior, R. J. Gelpi, J. C. Stupirski, A. Benatar, K. A. Gómez, C. Morales, A. Abbate, G. A. Rabinovich, Galectin-1 controls cardiac inflammation and ventricular remodeling during acute myocardial infarction. *Am. J. Pathol.* **182**, 29–40 (2013).
13. M. M. Bjørklund, A. K. Hollensen, M. K. Hagensen, F. Dagnaes-Hansen, C. Christoffersen, J. G. Mikkelsen, J. F. Bentzon, Induction of atherosclerosis in mice and hamsters without germline genetic engineering. *Circ. Res.* **114**, 1684–1689 (2014).
14. C. Wirth, U. Brandt, C. Hunte, V. Zickermann, Structure and function of mitochondrial complex I. *Biochim. Biophys. Acta* **1857**, 902–914 (2016).
15. A. W. Orr, N. E. Hastings, B. R. Blackman, B. R. Wamhoff, Complex regulation and function of the inflammatory smooth muscle cell phenotype in atherosclerosis. *J. Vasc. Res.* **47**, 168–180 (2010).
16. S. Allahverdian, C. Chaabane, K. Boukais, G. A. Francis, M. L. Bochaton-Piallat, Smooth muscle cell fate and plasticity in atherosclerosis. *Cardiovasc. Res.* **114**, 540–550 (2018).
17. R. C. Wirka, D. Wagh, D. T. Paik, M. Pjanic, T. Nguyen, C. L. Miller, R. Kundu, M. Nagao, J. Coller, T. K. Koyano, R. Fong, Y. J. Woo, B. Liu, S. B. Montgomery, J. C. Wu, K. Zhu, R. Chang, M. Alamprese, M. D. Tallquist, J. B. Kim, T. Quertermous, Atheroprotective roles of smooth muscle cell phenotypic modulation and the TCF21 disease gene as revealed by single-cell analysis. *Nat. Med.* **25**, 1280–1289 (2019).
18. V. Sorokin, K. Vickneson, T. Kofidis, C. C. Woo, X. Y. Lin, R. Foo, C. M. Shanahan, Role of vascular smooth muscle cell plasticity and interactions in vessel wall inflammation. *Front. Immunol.* **11**, 599415 (2020).
19. M. Liu, D. Gomez, Smooth muscle cell phenotypic diversity. *Arterioscler. Thromb. Vasc. Biol.* **39**, 1715–1723 (2019).
20. J. Shi, Y. Yang, A. Cheng, G. Xu, F. He, Metabolism of vascular smooth muscle cells in vascular diseases. *Am. J. Physiol. Heart Circ. Physiol.* **319**, H613–H631 (2020).
21. V. L. Thijssen, B. Barkan, H. Shoji, I. M. Aries, V. Mathieu, L. Deltour, T. M. Hackeng, R. Kiss, Y. Kloog, F. Poirier, A. W. Griffioen, Tumor cells secrete galectin-1 to enhance endothelial cell activity. *Cancer Res.* **70**, 6216–6224 (2010).
22. D. O. Croci, J. P. Cerliani, T. Dalotto-Moreno, S. P. Méndez-Huergo, I. D. Mascanfroni, S. Dergan-Dylon, M. A. Toscano, J. J. Caramelo, J. J. García-Vallejo, J. Ouyang, E. A. Mesri, M. R. Junttila, C. Bais, M. A. Shipp, M. Salatino, G. A. Rabinovich, Glycosylation-dependent lectin-receptor interactions preserve angiogenesis in anti-VEGF refractory tumors. *Cell* **156**, 744–758 (2014).
23. E. P. Moiseeva, Q. Javed, E. L. Spring, D. P. de Bono, Galectin 1 is involved in vascular smooth muscle cell proliferation. *Cardiovasc. Res.* **45**, 493–502 (2000).
24. Y. J. Lee, Y. S. Koh, H. E. Park, H. J. Lee, B. H. Hwang, M. K. Kang, S. Y. Lee, P. J. Kim, S. H. Ihm, K. B. Seung, K. Chang, Spatial and temporal expression, and statin responsiveness of galectin-1 and galectin-3 in murine atherosclerosis. *Korean Circ. J.* **43**, 223–230 (2013).
25. M. S. Tsai, M. T. Chiang, D. L. Tsai, C. W. Yang, H. S. Hou, Y. R. Li, P. C. Chang, H. H. Lin, H. Y. Chen, I. S. Hwang, P. K. Wei, C. P. Hsu, K. I. Lin, F. T. Liu, L. Y. Chau, Galectin-1 restricts vascular smooth muscle cell motility via modulating adhesion force and focal adhesion dynamics. *Sci. Rep.* **8**, 11497 (2018).
26. M.-T. Chiang, I.-M. Chen, F.-F. Hsu, Y.-H. Chen, M.-S. Tsai, Y.-W. Hsu, H.-B. Leu, P.-H. Huang, J.-W. Chen, F.-T. Liu, Y.-H. Chen, L.-Y. Chau, Gal-1 (galectin-1) upregulation contributes to abdominal aortic aneurysm progression by enhancing vascular inflammation. *Arterioscler. Thromb. Vasc. Biol.* **41**, 331–345 (2021).
27. J. Sénémaud, G. Caligiuri, H. Etienne, S. Delbosc, J. B. Michel, R. Coscas, Translational relevance and recent advances of animal models of abdominal aortic aneurysm. *Arterioscler. Thromb. Vasc. Biol.* **37**, 401–410 (2017).
28. G. Ailawadi, C. W. Moehle, H. Pei, S. P. Walton, Z. Yang, I. L. Kron, C. L. Lau, G. K. Owens, Smooth muscle phenotypic modulation is an early event in aortic aneurysms. *J. Thorac. Cardiovasc. Surg.* **138**, 1392–1399 (2009).
29. M. Roche-Molina, D. Sanz-Rosa, F. M. Cruz, J. García-Prieto, S. López, R. Abia, F. J. Muriana, V. Fuster, B. Ibáñez, J. A. Bernal, Induction of sustained hypercholesterolemia by single adeno-associated virus–mediated gene transfer of mutant hPCSK9. *Arterioscler. Thromb. Vasc. Biol.* **35**, 50–59 (2015).
30. A. Arbab-Zadeh, V. Fuster, From detecting the vulnerable plaque to managing the vulnerable patient: JACC state-of-the-art review. *J. Am. Coll. Cardiol.* **74**, 1582–1593 (2019).
31. C. K. Docherty, A. Carswell, E. Friel, J. R. Mercer, Impaired mitochondrial respiration in human carotid plaque atherosclerosis: A potential role for Pink1 in vascular smooth muscle cell energetics. *Atherosclerosis* **268**, 1–11 (2018).
32. C. Scheede-Bergdahl, A. Bergdahl, Adaptation of mitochondrial expression and ATP production in dedifferentiating vascular smooth muscle cells. *Can. J. Physiol. Pharmacol.* **95**, 1473–1479 (2017).
33. C. Bernal-Mizrachi, A. C. Gates, S. Weng, T. Imamura, R. H. Knutsen, P. DeSantis, T. Coleman, R. R. Townsend, L. J. Muglia, C. F. Semenkovich, Vascular respiratory uncoupling increases blood pressure and atherosclerosis. *Nature* **435**, 502–506 (2005).
34. J. Oller, E. Gabandé-Rodríguez, M. J. Ruiz-Rodríguez, G. Desdín-Micó, J. F. Aranda, R. Rodrigues-Diez, C. Ballesteros-Martínez, E. M. Blanco, R. Roldan-Montero, P. Acuña, A. Forteza Gil, C. E. Martín-López, J. F. Nistal, C. L. Lino Cardenas, M. E. Lindsay, J. L. Martín-Ventura, A. M. Briones, J. Miguel Redondo, M. Mittelbrunn, Extracellular tuning of mitochondrial respiration leads to aortic aneurysm. *Circulation* **143**, 2091–2109 (2021).
35. M. R. Bennett, S. Sinha, G. K. Owens, Vascular smooth muscle cells in atherosclerosis. *Circ. Res.* **118**, 692–702 (2016).
36. L. S. Shankman, D. Gomez, O. A. Cherepanova, M. Salmon, G. F. Alencar, R. M. Haskins, P. Swiatlowska, A. A. Newman, E. S. Greene, A. C. Straub, B. Isakson, G. J. Randolph, G. K. Owens, KLF4-dependent phenotypic modulation of smooth muscle cells has a key role in atherosclerotic plaque pathogenesis. *Nat. Med.* **21**, 628–637 (2015).

37. M. O. J. Grootaert, M. R. Bennett, Vascular smooth muscle cells in atherosclerosis: Time for a reassessment. *Cardiovasc. Res.* **117**, 2326–2339 (2021).
38. Z. Hu, W. Liu, X. Hua, X. Chen, Y. Chang, Y. Hu, Z. Xu, J. Song, Single-cell transcriptomic atlas of different human cardiac arteries identifies cell types associated with vascular physiology. *Arterioscler. Thromb. Vasc. Biol.* **41**, 1408–1427 (2021).
39. J. F. Bentzon, M. W. Majesky, Lineage tracking of origin and fate of smooth muscle cells in atherosclerosis. *Cardiovasc. Res.* **114**, 492–500 (2018).
40. X. Pang, J. Qiao, Galectin-1 inhibits PDGF-BB-induced proliferation and migration of airway smooth muscle cells through the inactivation of PI3K/Akt signaling pathway. *Biosci. Rep.* **40**, BSR20193899 (2020).
41. L. Zheng, C. Xu, Z. Guan, X. Su, Z. Xu, J. Cao, L. Teng, Galectin-1 mediates TGF-β-induced transformation from normal fibroblasts into carcinoma-associated fibroblasts and promotes tumor progression in gastric cancer. *Am. J. Transl. Res.* **8**, 1641–1658 (2016).
42. X. Zhu, K. Wang, K. Zhang, F. Xu, Y. Yin, L. Zhu, F. Zhou, Galectin-1 knockdown in carcinoma-associated fibroblasts inhibits migration and invasion of human MDA-MB-231 breast cancer cells by modulating MMP-9 expression. *Acta Biochim. Biophys. Sin.* **48**, 462–467 (2016).
43. J. K. Salabei, B. G. Hill, Mitochondrial fission induced by platelet-derived growth factor regulates vascular smooth muscle cell bioenergetics and cell proliferation. *Redox Biol.* **1**, 542–551 (2013).
44. L. Yang, L. Gao, T. Nickel, J. Yang, J. Zhou, A. Gilbertsen, Z. Geng, C. Johnson, B. Young, C. Henke, G. R. Gourley, J. Zhang, Lactate promotes synthetic phenotype in vascular smooth muscle cells. *Circ. Res.* **121**, 1251–1262 (2017).
45. T. X. Zhao, Z. Mallat, Targeting the immune system in atherosclerosis: JACC state-of-the-art review. *J. Am. Coll. Cardiol.* **73**, 1691–1706 (2019).
46. E. Lutgens, D. Atzler, Y. Döring, J. Duchene, S. Steffens, C. Weber, Immunotherapy for cardiovascular disease. *Eur. Heart J.* **40**, 3937–3946 (2019).
47. V. Sundblad, L. G. Morosi, J. R. Geffner, G. A. Rabinovich, Galectin-1: A jack-of-all-trades in the resolution of acute and chronic inflammation. *J. Immunol.* **199**, 3721–3730 (2017).
48. S. C. Starossom, I. D. Mascanfroni, J. Imitola, L. Cao, K. Raddassi, S. F. Hernandez, R. Bassil, D. O. Croci, J. P. Cerliani, D. Delacour, Y. Wang, W. Elyaman, S. J. Khoury, G. A. Rabinovich, Galectin-1 deactivates classically activated microglia and protects from inflammation-induced neurodegeneration. *Immunity* **37**, 249–263 (2012).
49. G. A. Rabinovich, G. Daly, H. Dreja, H. Tailor, C. M. Riera, J. Hirabayashi, Y. Chernajovsky, Recombinant galectin-1 and its genetic delivery suppress collagen-induced arthritis via T cell apoptosis. *J. Exp. Med.* **190**, 385–398 (1999).
50. M. J. Perone, S. Bertera, Z. S. Tawadrous, W. J. Shufesky, J. D. Piganelli, L. G. Baum, M. Trucco, A. E. Morelli, Dendritic cells expressing transgenic galectin-1 delay onset of autoimmune diabetes in mice. *J. Immunol.* **177**, 5278–5289 (2006).
51. V. Sundblad, I. A. Garcia-Tornadu, A. M. Ornstein, V. C. Martínez Allo, R. Lorenzo, S. G. Gatto, R. M. Morales, J. A. Gambarte Tudela, M. C. Manselle, D. O. Croci, D. Becu-Villalobos, G. A. Rabinovich, Galectin-1 impacts on glucose homeostasis by modulating pancreatic insulin release. *Glycobiology* **31**, 908–915 (2021).
52. H. Pan, C. Xue, B. J. Auerbach, J. Fan, A. C. Bashore, J. Cui, D. Y. Yang, S. B. Trignano, W. Liu, J. Shi, C. O. Ihuegbu, E. C. Bush, J. Worley, L. Vlahos, P. Laise, R. A. Solomon, E. S. Connolly, A. Califano, P. A. Sims, H. Zhang, M. Li, M. P. Reilly, Single-cell genomics reveals a novel cell state during smooth muscle cell phenotypic switching and potential therapeutic targets for atherosclerosis in mouse and human. *Circulation* **142**, 2060–2075 (2020).
53. C. E. Fernandez-García, C. Tarin, R. Roldan-Montero, D. Martinez-Lopez, M. Torres-Fonseca, J. S. Lindhot, M. Vega de Ceniga, J. Egido, N. Lopez-Andres, L. M. Blanco-Colio, J. L. Martín-Ventura, Increased galectin-3 levels are associated with abdominal aortic aneurysm progression and inhibition of galectin-3 decreases elastase-induced AAA development. *Clin. Sci.* **131**, 2707–2719 (2017).
54. A. I. Markowska, F. T. Liu, N. Panjwani, Galectin-3 is an important mediator of VEGF- and bFGF-mediated angiogenic response. *J. Exp. Med.* **207**, 1981–1993 (2010).
55. A. C. MacKinnon, X. Liu, P. W. Hadoke, M. R. Miller, D. E. Newby, T. Sethi, Inhibition of galectin-3 reduces atherosclerosis in apolipoprotein E-deficient mice. *Glycobiology* **23**, 654–663 (2013).
56. A. Marino, Y. Zhang, L. Rubinelli, M. A. Riemma, J. E. Ip, A. Di Lorenzo, Pressure overload leads to coronary plaque formation, progression, and myocardial events in ApoE$^{-/-}$ mice. *JCI Insight* **4**, e128220 (2019).
57. E. Gottfried, L. A. Kunz-Schughart, A. Weber, M. Rehli, A. Peuker, A. Müller, M. Kastenberger, G. Brockhoff, R. Andreesen, M. Kreutz, Expression of CD68 in non-myeloid cell types. *Scand. J. Immunol.* **67**, 453–463 (2008).
58. S. Allahverdian, A. C. Chehroudi, B. M. McManus, T. Abraham, G. A. Francis, Contribution of intimal smooth muscle cells to cholesterol accumulation and macrophage-like cells in human atherosclerosis. *Circulation* **129**, 1551–1559 (2014).
59. H. C. Stary, A. B. Chandler, S. Glagov, J. R. Guyton, W. Insull, Jr., M. E. Rosenfeld, S. A. Schaffer, C. J. Schwartz, W. D. Wagner, R. W. Wissler, A definition of initial, fatty streak, and intermediate lesions of atherosclerosis. A report from the Committee on Vascular Lesions of the Council on Arteriosclerosis, American Heart Association. *Circulation* **89**, 2462–2478 (1994).
60. P. Barrionuevo, M. Beigier-Bompadre, J. M. Ilarregui, M. A. Toscano, G. A. Bianco, M. A. Isturiz, G. A. Rabinovich, A novel function for galectin-1 at the crossroad of innate and adaptive immunity: Galectin-1 regulates monocyte/macrophage physiology through a nonapoptotic ERK-dependent pathway. *J. Immunol.* **178**, 436–445 (2007).
61. S. Martínez-Bartolomé, P. Navarro, F. Martín-Maroto, D. López-Ferrer, A. Ramos-Fernández, M. Villar, J. P. García-Ruiz, J. Vázquez, Properties of average score distributions of SEQUEST: The probability ratio method. *Mol. Cell. Proteomics* **7**, 1135–1145 (2008).
62. E. Bonzon-Kulichenko, F. Garcia-Marques, M. Trevisan-Herraz, J. Vazquez, Revisiting peptide identification by high-accuracy mass spectrometry: Problems associated with the use of narrow mass precursor windows. *J. Proteome Res.* **14**, 700–710 (2015).
63. F. Garcia-Marques, M. Trevisan-Herraz, S. Martinez-Martinez, E. Camafeita, I. Jorge, J. A. Lopez, N. Mendez-Barbero, S. Mendez-Ferrer, M. A. Del Pozo, B. Ibanez, V. Andres, F. Sanchez-Madrid, J. M. Redondo, E. Bonzon-Kulichenko, J. Vazquez, A novel systems-biology algorithm for the analysis of coordinated protein responses using quantitative proteomics. *Mol. Cell. Proteomics* **15**, 1740–1760 (2016).
64. I. Jorge, P. Navarro, P. Martinez-Acedo, E. Nunez, H. Serrano, A. Alfranca, J. M. Redondo, J. Vazquez, Statistical model to analyze quantitative proteomics data obtained by 18O/16O labeling and linear ion trap mass spectrometry: Application to the study of vascular endothelial growth factor-induced angiogenesis in endothelial cells. *Mol. Cell. Proteomics* **8**, 1130–1149 (2009).
65. P. Navarro, M. Trevisan-Herraz, E. Bonzon-Kulichenko, E. Nunez, P. Martinez-Acedo, D. Perez-Hernandez, I. Jorge, R. Mesa, E. Calvo, M. Carrascal, M. L. Hernaez, F. Garcia, J. A. Barcena, K. Ashman, J. Abian, C. Gil, J. M. Redondo, J. Vazquez, General statistical framework for quantitative proteomics by stable isotope labeling. *J. Proteome Res.* **13**, 1234–1247 (2014).
66. M. Trevisan-Herraz, N. Bagwan, F. García-Marqués, J. M. Rodriguez, I. Jorge, I. Ezkurdia, E. Bonzon-Kulichenko, J. Vázquez, SanXoT: A modular and versatile package for the quantitative analysis of high-throughput proteomics experiments. *Bioinformatics* **35**, 1594–1596 (2019).
67. D. W. Huang, B. T. Sherman, R. A. Lempicki, Bioinformatics enrichment tools: Paths toward the comprehensive functional analysis of large gene lists. *Nucleic Acids Res.* **37**, 1–13 (2009).
68. Y. Perez-Riverol, A. Csordas, J. Bai, M. Bernal-Llinares, S. Hewapathirana, D. J. Kundu, A. Inuganti, J. Griss, G. Mayer, M. Eisenacher, E. Pérez, J. Uszkoreit, J. Pfeuffer, T. Sachsenberg, S. Yilmaz, S. Tiwary, J. Cox, E. Audain, M. Walzer, A. F. Jarnuczak, T. Ternent, A. Brazma, J. A. Vizcaíno, The PRIDE database and related tools and resources in 2019: Improving support for quantification data. *Nucleic Acids Res.* **47**, D442–D450 (2019).
69. C. Gutiérrez-Muñoz, N. Méndez-Barbero, P. Svendsen, C. Sastre, V. Fernández-Laso, P. Quesada, J. Egido, J. C. Escolá-Gil, J. L. Martín-Ventura, S. K. Moestrup, L. M. Blanco-Colio, CD163 deficiency increases foam cell formation and plaque progression in atherosclerotic mice. *FASEB J.* **34**, 14960–14976 (2020).
70. V. Fernández-Laso, C. Sastre, N. Méndez-Barbero, J. Egido, J. L. Martín-Ventura, C. Gómez-Guerrero, L. M. Blanco-Colio, TWEAK blockade decreases atherosclerotic lesion size and progression through suppression of STAT1 signaling in diabetic mice. *Sci. Rep.* **7**, 46679 (2017).
71. N. B. Martin-Cofreces, F. J. Chichon, E. Calvo, D. Torralba, E. Bustos-Moran, S. G. Dosil, A. Rojas-Gomez, E. Bonzon-Kulichenko, J. A. Lopez, J. Otón, A. Sorrentino, J. C. Zabala, I. Vernos, J. Vazquez, J. M. Valpuesta, F. Sanchez-Madrid, The chaperonin CCT controls T cell receptor-driven 3D configuration of centrioles. *Sci. Adv.* **6**, eabb7242 (2020).

Acknowledgments: We thank L. Ortega Villanueva for technical assistance with immunohistochemical analysis and the support of P. Hockl. **Funding:** This study was funded by the Spanish MINECO (PID2019-106814RB-I00 and PGC2018-097019-B-I00), CAM (Complemento II-CM, S2017/BMD-3673), Fondo de Investigaciones Sanitarias ISCiii-FEDER [Biobancos RD09/0076/00101 and PRB3 (IPT17/0019, ProteoRed)], and FEDER "Una manera de hacer Europa." CIBERCV and CIBERDEM are Instituto de Salud Carlos III projects. This work also received funding from "La Caixa" Banking Foundation under the project code HR17-00247. The CNIC is supported by Instituto de Salud Carlos III (ISCIII), Ministerio de Ciencia, Innovación y Universidades (MCNU), and Pro CNIC Foundation and is a Severo Ochoa Center of Excellence (SEV-2015-0505). Further support was provided by Santander-UAM, Agencia Nacional de Promoción de la Investigación, el Desarrollo Tecnológico y la Innovación (PICT 2010-870, Argentina), Fundación Sales, and Fundación Bunge y Born (Argentina). We thank the support of Ferioli, Ostry, and Caraballo families. **Author contributions:** R.R.-M. performed in vivo experiments with models of atherosclerosis, immunohistochemistry, and in vitro studies. J.M.P.-S. produced and purified rGal-1 protein and contributed to analysis and discussion of the results. I.C.-P. performed proteomic studies and participated in the in vivo studies. J.O. performed in vitro experiments, analyzed data, and discussed results. D.M.-L. performed in vivo experiments with the AAA model. S.M.M., C.G.-M., and N.M.-B. contributed to in vivo

and in vitro studies. E.N. analyzed proteomics data. J.C.E.-G., J.-B.M., J.V., and M.M. analyzed data and discussed results. L.M.B.-C. performed experiments in models of atherosclerosis, analyzed data, and discussed results. G.A.R. and J.L.M.-V. conceived, designed, and supervised the study; analyzed data; and drafted the manuscript. All authors revised the final manuscript. **Competing interests:** The authors declare that they have no competing interests. **Data and materials availability:** All data needed to evaluate the conclusions in the paper are present in the paper and/or the Supplementary Materials. MS proteomics data have been deposited at the ProteomeXchange Consortium via the PRIDE partner repository with the dataset identifier PXD024637.

Submitted 7 October 2021
Accepted 25 January 2022
Published 16 March 2022
10.1126/sciadv.abm7322

ScienceAdvances

Galectin-1 prevents pathological vascular remodeling in atherosclerosis and abdominal aortic aneurysm

Raquel Roldán-MonteroJuan M. Pérez-SáezIsabel Cerro-PardoJorge OllerDiego Martinez-LopezEstefania NuñezSebastian M. MallerCarmen Gutierrez-MuñozNerea Mendez-BarberoJoan C. Escola-GilJean-Baptiste MichelMaria MittelbrunnJesús VázquezLuis M. Blanco-ColioGabriel A. RabinovichJose L. Martin-Ventura

Sci. Adv., 8 (11), eabm7322. • DOI: 10.1126/sciadv.abm7322

Science Advances (ISSN) is published by the American Association for the Advancement of Science. 1200 New York Avenue NW, Washington, DC 20005. The title *Science Advances* is a registered trademark of AAAS.